PNAS RESEARCH ARTICLE | IMMUNOLOGY AND INFLAMMATION OPEN ACCESS

Common inherited loss-of-function mutations in the innate sensor NOD2 contribute to exceptional immune response to cancer immunotherapy

Megan B. Barnet[a,b,c,d,1,2], Katherine J. L. Jackson[a,1], Etienne Masle-Farquhar[a], Amanda Russell[a], Deborah L. Burnett[a,e], Adrian Chye[a,b,c], Chris J. Jara[a,b], Megan Faulks[a], Amanda Mawson[a], Timothy J. Peters[a], Robert Brink[a,b], Katherine Wright[c], India Allen[a], Simon Junankar[a,b], Ian D. Davis[f,g,h], Gillian Heller[i], Zia Khan[j], Jeffrey Bruce[k], Cindy Yang[k], Stephenie Prokopec[k], Trevor Pugh[k], Andreas Behren[g,l,m], Georgina L. Hold[n], Fan Zhang[n], Wendy A. Cooper[o,p,q], Bo Gao[r,s], Adnan Nagrial[p,r,s], Anthony M. Joshua[a,b,c], Thomas John[t], Geoffrey Peters[u], Rina Hui[v], Michael Boyer[p,w], Prunella L. Blinman[p,x], Steven C. Kao[p,w], Jonathan Cebon[g,l,m,1], and Christopher C. Goodnow[a,b,e,1,2]

Affiliations are included on p. 11.

Contributed by Christopher C. Goodnow; received August 18, 2023; accepted May 21, 2025; reviewed by Tasuku Honjo and Alan J. Korman

Lung cancers and melanomas have many somatically mutated self-proteins that would be expected to trigger an immune rejection response, yet therapeutic responses can only be induced in a subset of patients. Here, we investigated the possibility that inherited differences in immune tolerance checkpoints contribute to variability in outcomes. Whole genome sequencing revealed biallelic germline loss-of-function (LOF) mutations in the immune tolerance checkpoint gene, *NOD2*, in an exceptional immune responder to targeted radiotherapy for metastatic melanoma. In 40 exceptional immune responders to anti-PD1 monotherapy for non–small cell lung cancer (NSCLC), genome sequencing showed 30% had inherited a *NOD2* LOF variant, more than twice the population frequency ($P = 0.0021$). Conversely, a gain-of-function *RIPK2* allele known to increase NOD2 signaling was inherited by 61% of nonresponders from the same cohort, compared to 10% of exceptional responders and much higher than the population frequency ($P < 0.0001$). Within the overall recruited cohort of 144 NSCLC anti-PD1 patients, individuals with immune-related adverse events (irAE) had better overall survival, further improved in those with *NOD2* LOF. In independent anti-PD1 monotherapy cohorts with a range of cancers, inherited *NOD2* LOF was associated with complete or partial response ($P = 0.0107$). Experimental validation in mice showed germline *Nod2* LOF enhanced therapeutic immune responses elicited by anti-PD1 monotherapy against a high mutation burden colorectal cancer, increasing tumor infiltration by effector memory CD8 T cells. Collectively these results reveal common inherited human variation in an immune tolerance checkpoint is a determinant of cancer immune responses elicited by pharmacological inhibition of another checkpoint.

cancer immunotherapy | immune checkpoint inhibitor | immune-related adverse event | inherited variant | autoimmune disease

Significance

These results help to explain, in part, the large variability in clinical response to a widely used cancer immunotherapy by revealing an inherited contribution from common functional variants in a single gene, *NOD2*. The results show that NOD2 is an important immune checkpoint not only for tolerating the gut microbiome but for human immune tolerance against cancer cells. The findings raise the possibility that *NOD2* genotyping may be useful as a predictive biomarker for anti-PD1 monotherapy of cancer, and that pharmacological inhibition of NOD2 signaling might improve therapeutic anticancer immunity.

A cooperating series of immune tolerance checkpoints strikes a balance between mounting potent immune responses to pathogens and the need for tolerance to self-tissues and commensal microbes (1). Immunotherapy with monoclonal antibodies against PD-1 or CTLA-4 blocks one checkpoint to break tolerance to cancer cell neoantigens and self-antigens (2). Nevertheless, even in tumors with a high mutational burden such as non–small cell lung cancer (NSCLC) in smokers, anti-PD1 checkpoint blockade provides a survival benefit in only a subset of patients, associated for some with induction of immune-related adverse events (irAEs) analogous to autoimmune diseases (3, 4).

In mouse genetic studies, breakdown of tolerance often requires a block in two or more checkpoints, illustrated by combined loss-of-function mutations in PD-1 and FAS (5), CBLB and AIRE (6), or *PTPN6*/SHP1, LYN, and CD22 (7). Based on these observations, here we test the hypothesis that inherited checkpoint defects cooperate with acute interventions such as PD-1 checkpoint blockade to promote exceptional immune response, defined here as a response observed in a small minority of treated patients.

Results

Abscopal Cancer and Autoimmune Response to Radiotherapy in an Exceptional Melanoma Patient. We considered germline defects in immune tolerance checkpoint genes initially in an exceptional patient case of melanoma, in whom complete tumor regression

Reviewers: T.H., Kyoto Daigaku; and A.J.K., Vir Biotechnology Inc.

Competing interest statement: C.C.G., M.B.B., J.C., A.B., and K.J.L.J. are included on a patent (International Publication Number WO 2020/223770); Cancer stratification and treatment based on inhibition of NOD-2. International application number: PCT/AU2020/050460, filed 8 May 2020. C.C.G. and M.B.B. have received research funding from Pfizer. W.A.C. has served on advisory boards for AstraZeneca, Amgen and Takeda. R.H. has received personal fees as an advisor and/or speaker from AstraZeneca, BMS, Eli Lilly, Merck, MSD, Novartis, Oncosec, Pfizer, Roche, and Seagen. S.C.K. has received personal fees as an advisor and/or speaker from BMS, MSD, Roche, AZ, Boeringher, Pfizer and Takeda.

Copyright © 2025 the Author(s). Published by PNAS. This open access article is distributed under Creative Commons Attribution-NonCommercial-NoDerivatives License 4.0 (CC BY-NC-ND).

[1]M.B.B., K.J.L.J., J.C., and C.C.G. contributed equally to this work.

[2]To whom correspondence may be addressed. Email: m.barnet@garvan.org.au or c.goodnow@garvan.org.au.

This article contains supporting information online at https://www.pnas.org/lookup/suppl/doi:10.1073/pnas.2314258122/-/DCSupplemental.

Published July 7, 2025.

Downloaded from https://www.pnas.org by 138.25.168.236 on January 11, 2026 from IP address 138.25.168.236.

occurred simultaneously with a flare of autoimmune colitis and subsequent vitiligo (Fig. 1*A*). Patient MEL1, a 51-y-old female, presented with poor-risk primary cutaneous malignant melanoma that was surgically excised. The patient's history was significant for an isolated episode of Crohn's colitis 15 y earlier, which resolved following oral corticosteroids without need for ongoing treatment. The patient developed multiple subcutaneous metastases 7 mo after primary excision, with supraclavicular lymphadenopathy, a 3 cm parenchymal liver lesion and 1.2 cm cerebral lesion. Biopsy of a subcutaneous lesion confirmed melanoma. Initial treatment was 18 gray stereotactic radiotherapy in a single fraction to the cerebral lesion. Weeks after radiotherapy, the patient required upper and lower endoscopy to investigate gastrointestinal bleeding. Colonoscopy showed colitis with acute inflammatory skip lesions consistent with Crohn's colitis. Oral prednisolone was commenced at 40 mg/day with good effect and weaned after 5 d.

During the 8 mo following cerebral radiotherapy and prior to commencement of systemic therapy, MEL1's subcutaneous lesions became impalpable and imaging showed resolution of liver and nodal lesions. The patient was observed off-treatment. A pathological fracture 28 mo after primary excision revealed an unrecognized isolated lytic lesion in the proximal humerus that was resected and treated with postoperative radiotherapy. Patches of vitiligo appeared at this time, progressing over the arms, face, and trunk in the ensuing months. The patient presented with upper abdominal pain 7 mo later, 3 y post primary excision, and underwent laparoscopic cholecystectomy. Large heavily pigmented masses were found in the neck of the gall bladder and cystic duct lymph node. Histopathology revealed melanin-laden macrophages only. Stains for S100 identified nerve bundles and scattered dendritic cells but no viable melanoma was found despite careful examination of numerous sections, including stains for gp100, MelanA/MART 1, and tyrosinase.

One subsequent melanoma relapse occurred 18 mo later, 4.5 y after primary excision, when the patient presented with symptoms of nasal obstruction and was found to have a nasopharyngeal mass. This was treated with resection and postoperative radiotherapy. Histological examination of the resected tissue revealed metastatic melanoma. The patient has since remained well, now beyond 20 y since last recurrence. She did not receive systemic therapy for melanoma at any point.

Abscopal response to radiotherapy is rare, occurring in less than 1 in 400 patients (8), and the conjunction with two autoimmune diseases posed the possibility that MEL1 might have an inherited tolerance checkpoint defect cooperating with radiotherapy-induced release of cancer antigens and inflammatory cytokines. Whole genome sequencing of DNA from blood for MEL1 (*SI Appendix*, Table S1) revealed compound heterozygous variants in *NOD2* (Fig. 1*B*): p.Leu1007ProfsTer2 (fs1007), carried by 2.6% of people in GnomAD; and p.Thr189Met carried independently by 0.51% of people in GnomAD; so that the expected frequency of compound heterozygosity is 1.3 in 10,000. *NOD2* loss-of-function variants are the strongest genetic risk factor for Crohn's disease with biallelic variants having the greatest effect (9, 10). The frameshift variant truncates the leucine-rich region of the NOD2 protein, completely impairing the innate sensing function of NOD2 to activate mitogen-activated protein kinase (MAPK) and NF-κB pathways within cells in response to bacterial cell wall component muramyl dipeptide (MDP), and increasing risk of Crohn's disease fourfold in heterozygotes (11–13). The T189M allele also significantly diminishes NOD2 signaling to NF-κB reporter genes (14). Exclusive carriage of one or other mutation within more than 1,000 individuals from the Medical Genome Reference Bank (MGRB) established the alleles segregate independently and are not in linkage disequilibrium (*SI Appendix*, Table S2) (15). Binding of NOD2 with its MDP ligand modulates immune gene expression through MAPK and NF-κB pathways, resulting in net stimulatory or suppressive effects dependent on dose, timing, duration, and route of MDP exposure (16–18). While the mechanism is unresolved, NOD2 serves as an important checkpoint for tolerance to commensal gut microbes.

Cancer and Autoimmune Responses in a Large Cohort of Exceptional Responders to Lung Cancer Immunotherapy. Since abscopal cancer immune responses of this magnitude are rare, we next tested for inherited *NOD2* pathway defects in a clinical setting where therapeutic immune responses are more frequently elicited, albeit still in the minority of cases. Melanoma and NSCLC were the only common cancers routinely treated with single-agent anti-PD1 in 2017, and treatment outcomes were significantly worse for (PD-L1 nonselected) NSCLC than for melanoma, with 2-y

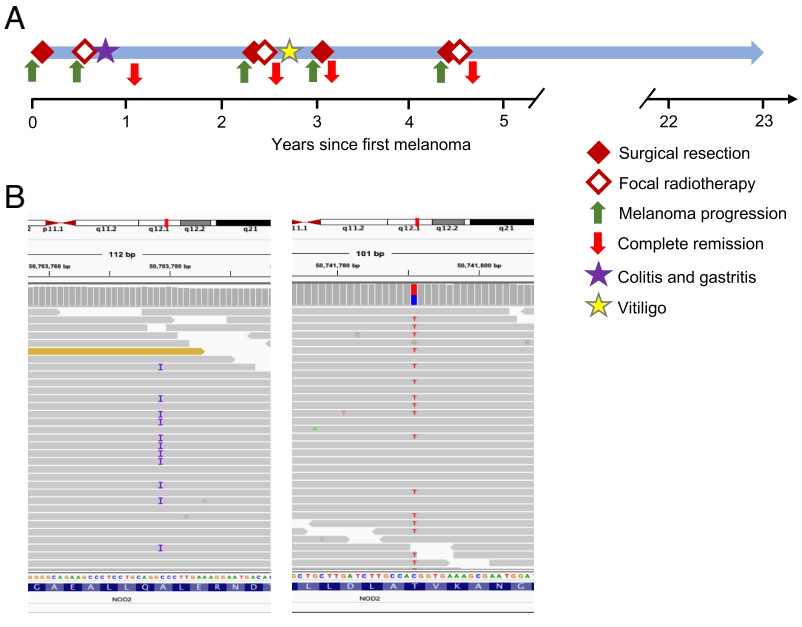

Fig. 1. Exceptional immune response to metastatic melanoma triggered by irradiation of a cerebral tumor in patient case MEL1. (*A*) Course of disease. Key shows treatment, tumor status, type of immune related adverse event. (*B*) Results of whole genome sequencing showing (*Left*) p.Leu1007ProfsTer2 (rs2066847) and (*Right*) p.Thr189Met (rs61755182).

Downloaded from https://www.pnas.org by 138.25.168.236 on January 11, 2026 from IP address 138.25.168.236.

overall survival (OS) rates of 23 and 55% respectively(19, 20). We therefore recruited patients with metastatic NSCLC, because selection of exceptionally good treatment outliers over a fixed time period was more feasible in this cohort.

From 742 patients with NSCLC treated with single agent anti-PD-1/PD-L1 at multiple hospitals in Sydney, Australia, 144 patients were enrolled with a focus on capturing long-term responders (Fig. 2). Of eligible patients, 56% were male, 87% were current or former smokers and 63.6% received anti-PD1/PD-L1 in the 2nd or subsequent line (*SI Appendix*, Table S3). Patients received treatment either on trial [ClinicalTrials.gov, NCT01905657(21)], through a pharma-funded access program, or as standard treatment following Pharmaceutical Benefits Advisory Committee recommendation for PBS-funding in July 2019 (22). For all 144 enrolled individuals in the cohort, DNA prepared from peripheral blood mononuclear cells was genotyped on Axiom Precision Medicine Diversity arrays for ~850,000 common inherited single nucleotide polymorphisms (SNPs).

To test the hypothesis that inherited tolerance checkpoint defects might increase cancer therapeutic response and autoimmune adverse events, exceptional immune response was defined as progression free survival (PFS) of at least 2 y on single-agent anti-PD1/PDL1—representing only 12% of patients within the Checkmate 057 clinical trial (19) - AND development of at least one Common Terminology Criteria for Adverse Events (CTCAE) grade ≥2 irAE at any point during treatment. From the 144 patients enrolled, 40 patients meeting these criteria were analyzed by germline whole genome sequencing (WGS) to identify rare and common inherited variants (Fig. 2). Seven of the 40 exceptional responder patients (17.5%) had a previous diagnosis of an autoimmune condition, although none had a history of Crohn's disease (*SI Appendix*, Table S4).

As an internal control, a group of patients who gained no clinical benefit from treatment was also selected from the recruited cohort of 144 individuals. Nonresponders were defined by 3 criteria: 1) best response of progressive disease; 2) treatment duration of at least 2 mo *or* 3 doses (whichever is longer); and 3) overall survival of ≤ 24 mo. Eighteen patients with treatment nonresponse were selected for WGS, 3 of whom had previous diagnosis of an autoimmune condition (16.67%) (Fig. 2, *SI Appendix*, Table S4).

For the 40 individuals in the exceptional immune responder group, complete or partial response was observed in 38 patients (95%), with prolonged stable disease in the remaining 2 patients (Fig. 3). The median follow-up was 41 mo from drug commencement (range 24+ to 95+ mo). Because of the low rates of progression and death, neither the median PFS nor median overall survival (OS) for the entire exceptional responder cohort could be computed at data cut-off. Five of 40 patients (7.5%) had progressed on treatment, with median PFS of 37 mo (95% CI, 16.9 to 57.1). Four of these patients were deceased, with median OS of 39 mo (95% CI, 20.8 to 53.2). Per inclusion criteria, 2-y PFS was 100%. Pooled data from comparable second-line trials show median PFS of 2.56 mo and OS of 11.1 mo, with 13% of patients remaining progression-free at 2 y (23). Of the exceptional responder patients, 50% had one irAE, 30% had two, and 20% had three or more irAEs (Fig. 3 and *SI Appendix*, Table S4).

Within the 18 individuals in the nonresponder group, all patients had progressive disease as best response and all were deceased at the time of analysis (*SI Appendix*, Fig. S1). The median PFS was 2.76 mo (95% CI, 2.1-3.81), the median OS 11.085 mo (95% CI, 5.98 to 14.95), and 3 patients each had one documented irAE (*SI Appendix*, Fig. S1 and Table S4).

Increased Frequency of *NOD2* Loss-of-Function in Lung Cancer Immunotherapy Exceptional Responders. Based on the findings in MEL1, germline whole genome sequences from patients with NSCLC and exceptional response or nonresponse to anti-PD1 treatment were analyzed for a set of 33 human inherited *NOD2* loss of function (LOF) variants that have previously been demonstrated experimentally to impair NOD2 signaling to

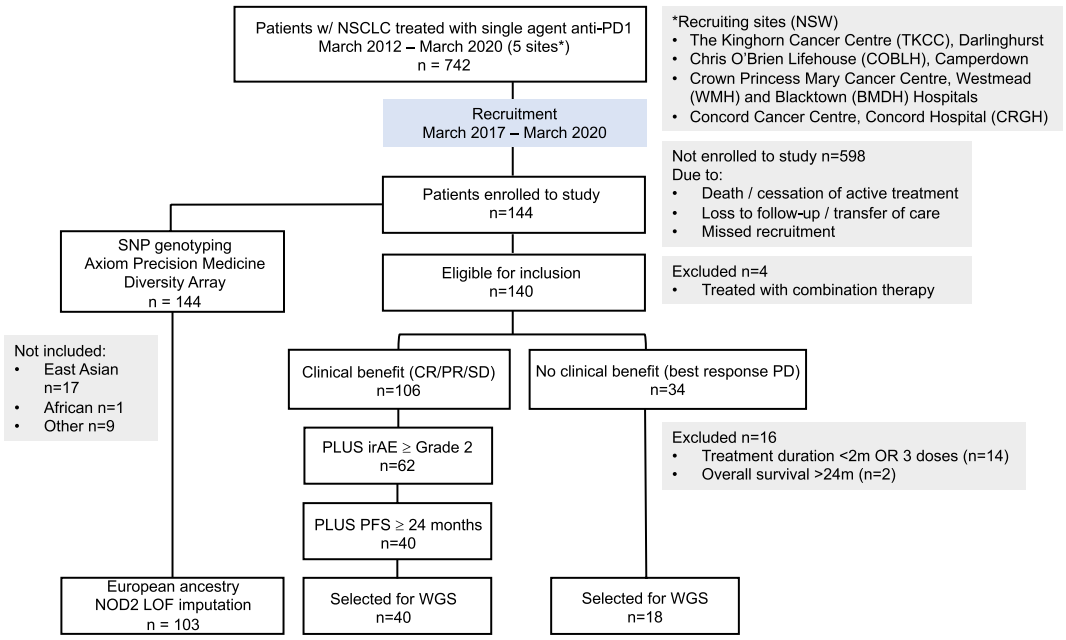

Fig. 2. Study profile to test interaction between anti-PD1 blockade and inherited immune genotype. Of 742 patients treated with single-agent anti-PD1 for NSCLC between March 2012-March 2017 per pharmacy administration records, 144 patients were enrolled to the study with a focus on presumptive exceptional responders (n = 106). DNA from all 144 enrolled individuals was profiled for common inherited polymorphisms by SNParray, and *NOD2* loss-of-function (LOF) variants called or imputed in those of European ancestry. 40 patients meeting the exceptional response criteria of clinical benefit AND at least 1 irAE≥ grade 2 AND PFS ≥ 24 mo were analyzed by whole genome sequencing of germline (blood) DNA. 34 patients were identified who gained no clinical benefit; 14 were excluded due to insufficient treatment duration (<2 m OR 3 doses), 2 were excluded due to OS>24 m, and the remaining 18 cases underwent whole genome sequencing. irAE: immune-related adverse-event; PFS: progression free survival; WGS: whole genome sequencing; OS: overall survival.

Downloaded from https://www.pnas.org by 138.25.168.236 on January 11, 2026 from IP address 138.25.168.236.

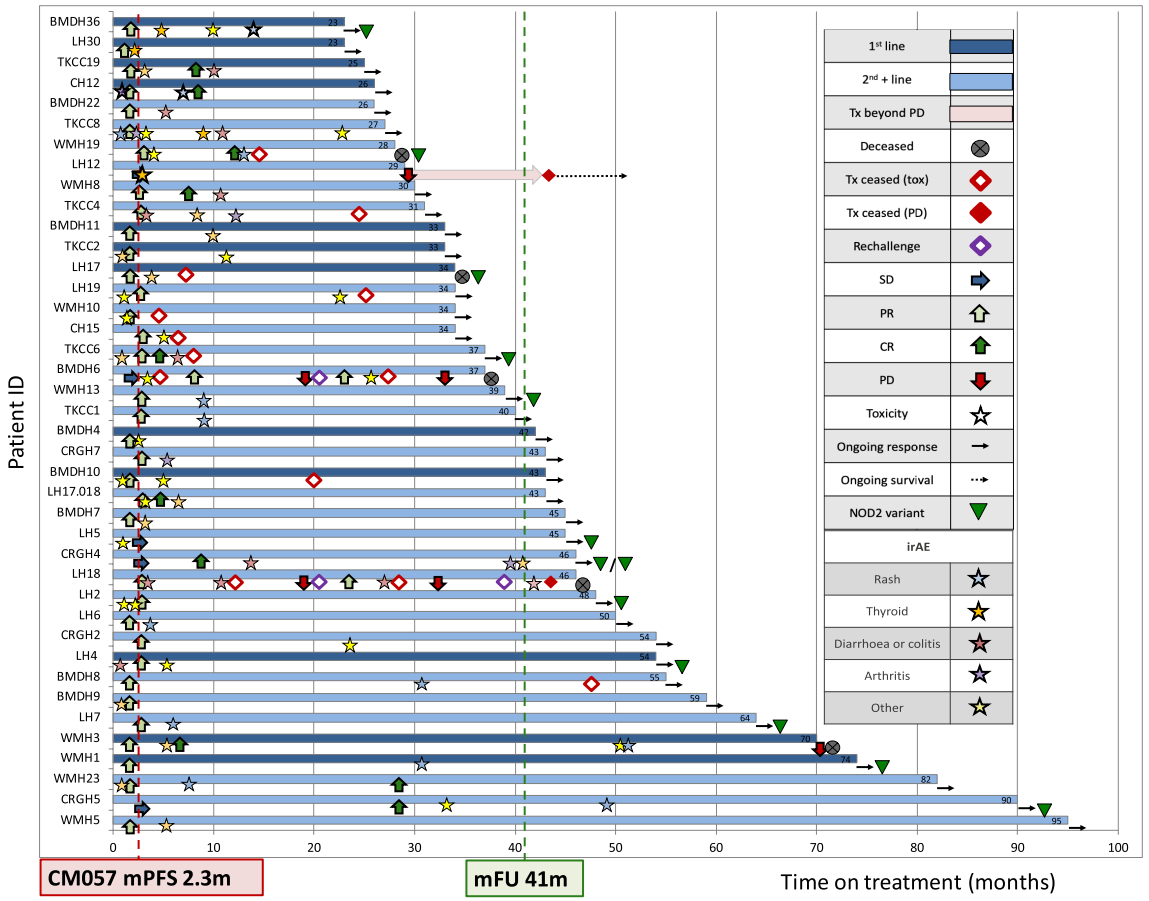

Fig. 3. Exceptional immune response to metastatic NSCLC triggered by anti-PD1 monotherapy. Swimmer plot showing course of disease following treatment with anti-PD1 in 40 exceptional immune responder patients and median follow up (mFU, green dashed line), compared to the median PFS in patients on the Checkmate-057 trial (CM057 mPFS, red dashed line). Key shows treatment & patient status, response type (SD, stable disease; PR, partial response; CR, complete response; PD, progressive disease), type of immune related adverse event (irAE); tox: toxicity; Tx: treatment.

NF-κB reporter genes (9, 10, 14, 24–26) (Table 1). We compared the observed frequency in exceptional immune responders and nonresponders with the expected allele frequencies derived from gnomAD (27). Twelve patients (30%) in the exceptional immune responder cohort carried one or more functional *NOD2* LOF variants, totaling 13 of 80 *NOD2* alleles (16.25%); significantly higher than the expected allele count of 5.27 and predicted allele frequency of 6.58% ($P = 0.0021$). One patient had biallelic *NOD2* LOF and developed three irAEs during treatment, compared to 11 patients with monoallelic LOF variants where 6 had a single irAE, 3 had two irAEs, one had three and one had four irAEs (*SI Appendix*, Table S4). The number of individuals is nevertheless insufficient to conclude whether or not biallelic *NOD2* LOF increases the risk of anti-PD1 induced irAEs, as it does for the risk of spontaneous Crohn's disease. *NOD2* LOF variants were found in patients with nonsquamous disease (*SI Appendix*, Table S5). The number and types of irAEs in patients with *NOD2* LOF variants appeared similar to patients with wild-type *NOD2* (*SI Appendix*, Table S6). Specifically, all-grade diarrhea events (including biopsy confirmed colitis) occurred in 13.6% of patients with or without *NOD2* LOF variants, although the total number of cases with this irAE (n = 9) is too small to draw conclusions.

Within nonresponders, one patient carried a single *NOD2* LOF allele, totaling 1 out of 36 alleles (2.78%): lower than the AF in exceptional responders (16.25%, $P = 0.02$) and in gnomAD (6.58%, $P = 0.4$), noting the small sample size of nonresponders available.

Higher than expected frequency of *NOD2* LOF variants in the exceptional immune responder cohort could reflect a genetic contribution to lung cancer risk, population stratification, or differences in the computational pipelines. To test the former, we interrogated The Cancer Genome Atlas (TCGA) lung adenocarcinoma (LUAD) cohort for the three most common *NOD2* LOF variants, together comprising over 80% of disease-causing variants and each known to independently impair protein function; G908R, R702W, and fs1007 (9, 10, 24, 25, 28). The pooled allele frequencies (AF) for these variants remained higher within exceptional responders than both gnomAD (13.75% vs 5.2%, $P = 0.0028$) and TCGA-LUAD (13.75% vs 7.1%, $P = 0.045$) (*SI Appendix*, Table S7). With respect to population stratification, our patients were selected from the greater Sydney region, enriching for European ethnicity which comprised 82.5% of the cohort using the Ancestry and Kinship Tookit (29). To test the impact of stratification and computational pipelines, we compared our results to the Medical Genome Reference Bank (MGRB); a data resource of ~3,000 well elderly Australians predominantly of European descent whose WGS was analyzed by the same sequencing facility and computational pipeline used for the exceptional responders (15). The combined allele frequencies of the three LOF *NOD2* alleles was higher within exceptional responders compared with MGRB (13.75% vs 7.5%, $P = 0.05$) (*SI Appendix*, Table S7).

Signaling by NOD2 is dependent on MDP phosphorylation by *N*-acetylglucosamine kinase (*NAGK*) (30), and on NOD2 binding with receptor-interacting protein kinase 2 (*RIPK2*) leading to recruitment of the ubiquitin E3 ligase X-chromosome-linked inhibitor of apoptosis (*XIAP*) (31). We therefore evaluated variants in these essential genes in the exceptional responders and nonresponders. Primary deficiency in *XIAP* is rare and has variable manifestations including inflammatory bowel disease (32). No functional variants within *XIAP* were found in either cohort. Two individuals, both exceptional responders, carried rare *NAGK* missense variants: p.N173H rs1022300452 and p.Y183H rs139590364. We draw no conclusions from these variants since their functional consequence is unknown.

Downloaded from https://www.pnas.org by 138.25.168.236 on January 11, 2026 from IP address 138.25.168.236.

Table 1. Germ-line *NOD2* loss-of-function in large cohort of exceptional responders to lung cancer immunotherapy analyzed by whole genome sequencing

HGVS protein change	rsID	Gnomad wt allele count	Gnomad LoF allele count	Expected AF	Observed AF (n = 80)	Expected allele count EX RES	Observed allele count EX RES	Expected allele count NON RES	Observed allele count NON RES
R38M	rs104895487	282455	17	6.02E-05	0	4.82E-03		2.17E-03	
R138Q	rs104895456	282161	25	8.86E-05	0	7.09E-03		3.19E-03	
W157R	rs104895420	281750	34	1.21E-04	0	9.66E-03		4.35E-03	
V162I	rs45575333	281027	29	1.03E-04	0	8.24E-03		3.71E-03	
T189M	rs61755182	282251	651	2.30E-03	0	1.84E-01		8.28E-02	
R235C	rs104895422	282820	32	1.13E-04	0	9.05E-03		4.07E-03	
L248R	rs104895423	282617	147	5.20E-04	1.25E-02	4.16E-02	1	1.87E-02	
N289S	rs5743271	281118	1246	4.41E-03	1.25E-02	3.53E-01	1	1.59E-01	
D291N	rs104895424	282357	3	1.06E-05	0	8.50E-04		3.82E-04	
L349V	rs752615209	251426	2	7.96E-06	0	6.36E-04		2.86E-04	
W355.	rs104895488	251415	1	3.98E-06	0	3.18E-04		1.43E-04	
I363F	rs104895470	251462	12	4.77E-05	0	3.82E-03		1.72E-03	
S431L	rs104895431	281874	268	9.50E-04	0	7.60E-02		3.42E-02	
E441K	rs104895432	281643	93	3.30E-04	0	2.64E-02		1.19E-02	
P463A	rs104895482	0	0	0.00E+00	0	0.00E+00		0.00E+00	
L550V	rs104895471	0	0	0.00E+00	0	0.00E+00		0.00E+00	
558delLG	rs1407856583	249116	2	8.03E-06	0	6.42E-04		2.89E-04	
A612T	rs104895438	282597	169	5.98E-04	0	4.78E-02		2.15E-02	
A612V	rs104895439	251382	4	1.59E-05	0	1.27E-03		5.73E-04	
R702W	rs2066844	272720	7242	2.59E-02	5.00E-02	2.07E+00	4	9.32E-01	
R713C	rs104895440	248895	3	1.21E-05	0.00E+00	9.64E-04		4.34E-04	
A755V	rs61747625	281563	711	2.52E-03	0	2.02E-01		9.07E-02	
E778K	rs104895443	282362	66	2.34E-04	0	1.87E-02		8.42E-03	
E843K	rs104895445	282725	23	8.13E-05	0	6.51E-03		2.93E-03	
R790W	rs62029861	281223	23	8.18E-05	0	6.54E-03		2.94E-03	
N825K	rs104895485	251363	1	3.98E-06	0	3.18E-04		1.43E-04	
A849V	rs104895486	251128	20	7.97E-05	0	6.38E-03		2.87E-03	
N852S	rs104895467	282589	309	1.09E-03	0	8.74E-02		3.93E-02	
W907R	rs104895490	251453	1	3.98E-06	0	3.18E-04		1.43E-04	
G908R	rs2066845	279765	3081	1.09E-02	5.00E-02	8.72E-01	4	3.92E-01	
fs1007	rs199883290	278464	4298	1.52E-02	3.75E-02	1.22E+00	3	5.47E-01	1
L1007P	rs2066847	251391	1	0.00E+00	0	0.00E+00		0.00E+00	
R1019.	rs104895491	282552	6	2.12E-05	0	1.70E-03		7.63E-04	
Total		262939	18520	0.07	0.16	5.27	13	2.37	1
					**P = 0.0021				

Expected versus observed frequency of inherited NOD2 variants that have previously been experimentally demonstrated to be loss-of-function (LOF), in patients with NSCLC and exceptional immune response (EX RES) or nonresponse (NON-RES) to anti-PD1. Allele counts and expected allele frequency (AF) in the genome aggregation database (gnomAD) and in the 40 exceptional immune responders and 18 nonresponders. *P* value by two-tailed Fisher's exact test.

By contrast, a p.Ile259Thr *RIPK2* variant (rs2230801) that hyperactivates signaling, is associated with Behçets Disease (33, 34), and would be expected to have the opposite effect to *NOD2* LOF, was carried by 11 of 18 nonresponders (61.1%) totaling 12 of 36 alleles (33.3%). The hypersignaling *RIPK2* allele frequency was significantly higher in nonresponders than in exceptional responders (5%, $P = 0.0001256$) or in the general population (6.9%, $P < 0.0001$) (*SI Appendix*, Table S7).

Immune-Related Adverse Events and Inherited Immune Genotype Predict Survival. While the results above employed whole genome sequencing to detect inherited rare and common variants in the exceptional and nonresponder groups, we also employed genome-wide SNP array genotyping for common inherited variants in each of the 144 anti-PD1/PDL1 treated NSCLC patients enrolled in the study (Fig. 2). This enabled calling or imputation of inherited common *NOD2* loss-of-function variants, the *RIPK2* gain-of-function variant, and common variants across the genome that contribute to susceptibility to different autoimmune diseases in genome-wide association studies. Since the latter have primarily studied autoimmune susceptibility in people of European ancestry, we focused on the 103 enrolled individuals with this ancestry as defined by multidimensional scaling (MDS) using 1,000 genome reference. In these individuals, we asked whether or not *NOD2* LOF variants contribute to lung cancer survival in anti-PD-1 treated individuals in concert with occurrence of irAEs or polygenic risk of autoimmune disease resulting from inherited common variants linked to genes for many different immune checkpoints.

Occurrence of irAEs correlated strongly with improved survival across the recruited cohort (median OS 48 versus 17 mo, $P = 2 \times 10^{-8}$) (*SI Appendix*, Fig. S2). Individuals of European ancestry with inherited *NOD2* LOF and irAE tended to survive best, whereas those without an irAE but inherited *NOD2* LOF had the poorest

Downloaded from https://www.pnas.org by 138.25.168.236 on January 11, 2026 from IP address 138.25.168.236.

survival ($P = 3 \times 10^{-7}$; Fig. 4*A*). Of polygenic risk scores for 10 autoimmune diseases examined (*SI Appendix*, Table S8), only the score for psoriasis significantly separated survival in concert with *NOD2* LOF ($P = 0.02$, Fig. 4*B*). Collectively, these results suggest complex interactions between irAEs, inherited immune genotype, and NSCLC survival following anti-PD1/PDL1 blockade.

Association of *NOD2* Loss-of-Function with Immunotherapy Response in Independent Mixed Cancer Cohorts. To investigate *NOD2* loss-of-function variants in independent cohorts treated with single agent anti-PD1/PD-L1 for a range of cancer types, we analyzed germline exome sequencing results from nine studies deposited in dbGaP (*SI Appendix*, Table S9) and whole exome germline sequencing from the Princess Margaret Cancer Centre INSPIRE basket trial cohort (35) (*SI Appendix*, Table S10). As a complement to the exceptional responder cohort analyzed above, the pooled dbGAP/INSPIRE cohort (Table 2) had the advantage that exome data was available with germline *NOD2* sequence coverage for most of the treated cohort regardless of response, but the disadvantage that the treated cohort was smaller (n = 160 compared to n = 742) and no information on irAEs was available for dbGaP patients.

In the dbGaP/INSPIRE cohort, 18 individuals harbored a *NOD2* LOF variant (11.3%, Table 2). Patients harboring a *NOD2* LOF variant had higher response rate than their wild type counterparts (ORR 56% versus 25%, $P = 0.0107$), and *NOD2* LOF variants were disproportionately high within complete (33.3%) and partial (19%) responders, compared with stable (6%) and progressive (8%) disease ($P = 0.0402$). Survival data were incompletely annotated in dbGaP, but progression-free and overall survival favored patients with *NOD2* LOF within INSPIRE, without reaching statistical significance (PFS 7.9 versus 2.4 mo, $P = 0.12$; OS 19 versus 13.9 mo, $P = 0.4$). Data for irAEs were available for patients within INSPIRE. Among evaluable patients who experienced an irAE (n = 24), 27% of responders and 0% of nonresponders carried a NOD2 LOF variant whereas among those without an irAE (n = 76) 14% of responders and 6% of nonresponders carried NOD2 LOF (*SI Appendix*, Table S11). In addition to validating the findings in the larger cohort of NSCLC exceptional responders above, these results highlight the unique attributes of the exceptional responders cohort: integrating irAEs with cancer response, and drawing upon a 4.6 times larger base of anti-PD1/PDL1 monotherapy-treated patients.

NOD2 Loss-of-Function Enhances Response to Immunotherapy in Mice. As further validation of the association between inherited *NOD2* LOF and improved cancer response to anti-PD1, we analyzed genetically homogeneous mice transplanted with a syngeneic tumor carrying a high mutation burden. The three most prevalent human *NOD2* variants (G908R, R702W, and fs1007) have been experimentally demonstrated to cause profound loss of function (9, 10, 24, 25). We therefore used CRISPR-*Cas9* to create a loss-of-function *Nod2* allele in C57BL/6 J mice by generating a frameshift mutation ($Nod2^{fs}$) truncating the protein (*SI Appendix*, Fig. S3). $Nod2^{fs}$ C57BL/6 J mice demonstrated complete impairment of NOD2 signaling (*SI Appendix*, Fig. S4) and had no overt phenotype. We focused on homozygous loss-of-function based on the observation that Crohn's disease is much more frequent in people with biallelic *NOD2* loss of function and the observation that dysregulated immunity due to inherited loss-of-function in other checkpoint genes such as *TNFAIP3* and *CTLA4* is haploinsufficient in humans but recessive in mice.

To test the cancer response to PD-1 checkpoint inhibition, we transplanted $Nod2^{fs}$ and $Nod2^{wt}$ C57BL/6 J mice subcutaneously with the colonic adenocarcinoma cell line, MC38 (36). This transplantable tumor is known to have a high tumor mutation burden from *Msh3* and *Pold1* mutations and, in syngeneic C57BL/6 recipients, elicits a partial response with anti-PD1 monoclonal antibody treatment (37–41). Once transplanted tumors were established, mice were treated with a monoclonal antibody against PD-1 that blocks binding to PDL1 and PDL2.

Inhibition of MC38 tumor growth following commencement of anti-PD-1 was greater in the $Nod2^{fs}$ cohort (Fig. 5*A* and *SI Appendix*, Fig. S5*A*), with 60-d overall survival of 10.5% compared with 0% in $Nod2^{wt}$ mice (Fig. 5*B*). In mice treated with control IgG there was no significant difference in tumor growth between $Nod2^{fs}$ and $Nod2^{wt}$ animals. Upon anti-PD1 treatment a similar trend was observed in C57BL/6 J $Nod2^{fs}$ mice transplanted with an alternative, less immunogenic syngeneic tumor cell-line, AT-3, although this did not reach statistical significance (*SI Appendix*, Fig. S5 *B* and *C*). We did not observe clinical evidence for irAEs in the anti-PD-1 treated $Nod2^{fs}$ mice (normal fecal pellets, stable body weight, normal behavior), although as noted above in the human cohort there were comparable frequencies of irAEs in patients with or without *NOD2* LOF variants.

Flow cytometry of tumor tissue and spleen cells after two (T1) or four (T2) doses of anti-PD1 (Fig. 5 and *SI Appendix*, Fig. S6) revealed tumor infiltrating CD8+ and CD4+ T cells were increased as a % of live cells at the T1 timepoint in $Nod2^{fs}$ mice but not significantly different at T2 (Fig. 5 *C* and *E*). Tumors in $Nod2^{fs}$ animals contained more CD8+ $CD44^{hi}$ $CD62L^{low}$ effector memory cells as a % of CD8+ cells at both timepoints (Fig. 5*D*). $CD4^{+}$ $CD25^{hi}$ $CD127^{low}$ T cells were increased and may represent Treg cells responding to

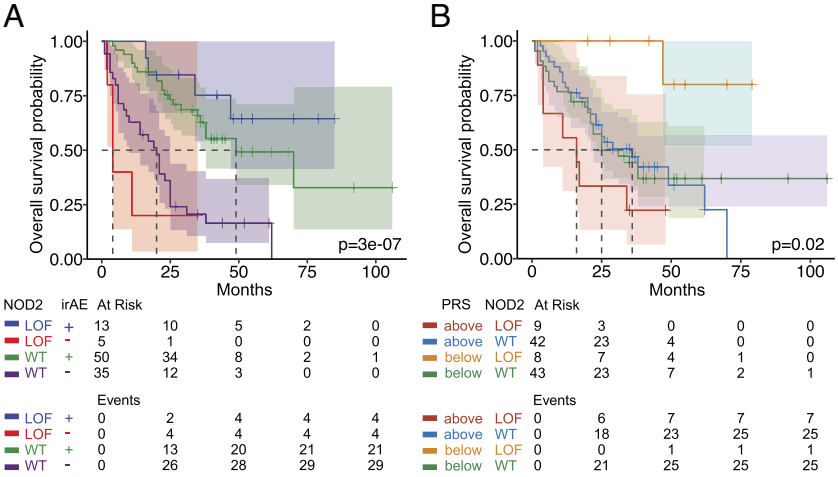

Fig. 4. irAEs and inherited immune genotype correlate with survival in metastatic NSCLC treated with anti-PD1 monotherapy. Kaplan–Meier survival curves for 103 individuals of European ancestry and imputed *NOD2* genotype in the enrolled cohort of 144 patients analyzed by SNParray, separated into 4 groups according to: (*A*) individuals with (+) or without (−) irAE and *NOD2* LOF or wildtype (WT) genotype; (*B*) individuals with above or below median polygenic risk score (PRS) for psoriasis and *NOD2* LOF or wildtype genotype. Numbers of individuals at risk at time 0 and at the indicated times on treatment are shown. Survival curves compared by log-rank (chi squared) test with three degrees of freedom; shading indicates 95% CI. irAEs; immune-related adverse events, LOF; loss of function.

Downloaded from https://www.pnas.org by 138.25.168.236 on January 11, 2026 from IP address 138.25.168.236.

Table 2. Germline *NOD2* loss-of-function in pooled cohort of exome sequenced cancer patients with varying response to immunotherapy

INSPIRE & dbGaP: RECIST1.1 BEST OVERALL RESPONSE	*NOD2* LOF	*NOD2* WT	% pts *NOD2* LOF
CR	3	6	33%
PR	7	30	19%
SD	3	47	6%
PD	5	59	8%
Fisher's exact one-tailed *P* =	0.04021		
Responded (CR+PR)	10	36	22%
No response (PD + SD)	8	106	7%
Overall Response Rate	56%	25%	
Fisher's exact one-tailed *P* =	0.01066		

Combined data for RECIST response type (*Top*) and overall response rate (ORR, *Bottom*) according to NOD2 genotype. Data from informative patients treated with single-agent anti-PD1/PD-L1 for a range of cancer types with progression-free survival >60 days and germline exome sequence coverage of NOD2 (n = 160) in dbGaP and INSPIRE cohorts. Combined cohorts; 40 NSCLC, 13 melanoma, 13 bladder cancer, 23 head and neck squamous cell carcinoma, 20 ovarian cancer, 19 breast cancer, 32 other cancers. CR, complete response; PR, partial response; SD, stable disease; PD, progressive disease. LOF, individuals carrying at least one NOD2 allele that is loss-of-function based on previous experimental evidence; WT, individuals with both NOD2 alleles wild-type. p-values by one-tailed Fisher's exact test.

increased inflammation, although in the absence of intracellular FoxP3 staining these could also represent activated CD4+ cells. After gating out $CD25^{hi}$ $CD127^{low}$ cells, CD4+ $CD44^{hi}$ $CD62L^{low}$ effector T cells were decreased in $Nod2^{fs}$ tumors as a % of CD4+ cells at T2 (Fig. 5 *F* and *G*). By contrast, there were no significant differences in the % of these T cell subsets in the spleen of $Nod2^{fs}$ and $Nod2^{wt}$ animals at either timepoint (*SI Appendix*, Fig. S6 *A–G*).

The % of CD11c+ CD11b- dendritic cells among live tumor cells was not significantly different between the genotypes (*SI Appendix*, Fig. S6 *K* and *L*) although the % of CD8+ cells among these dendritic cells was increased in $Nod2^{fs}$ mice at T1 (*SI Appendix*, Fig. S6*M*). $Ly6G^{hi}$ CD11b+ cells, comprising neutrophils and granulocytic myeloid-derived suppressor cells, were increased as a % of live tumor cells in $Nod2^{fs}$ mice at T2 (*SI Appendix*, Fig. S6*O*). Thus, despite the $NOD2^{fs}$ mutation disrupting macrophage production of the mouse IL-8 homologue KC (*SI Appendix*, Fig. S4), there was no disruption of recruitment to the tumor of cells with a granulocytic myeloid-derived suppressor cell phenotype. There was also no detectable difference in F4/80+ CD11b+ Ly6G- macrophages as a % of live cells in the tumors of $Nod2^{fs}$ and $Nod2^{wt}$ animals (*SI Appendix*, Fig. S6*P*).

Given the greater tumor infiltration with CD8+ effector T cells in $Nod2^{fs}$ animals, we considered the possibility that *NOD2* peptides presented on MC38 cells might be recognized as foreign antigens in $Nod2^{fs}$ mice, similar to the neoantigens generated by cancer somatic mutations. This possibility appears unlikely based on two observations in previously published data. First, MC38 cells express very low levels of *Nod2* mRNA, 39 times lower than the average of mRNAs encoding immunogenic neoantigen peptides on these cells (40). Moreover, among 6,239 different peptides identified as bound to MHC I on MC38 cells none were derived from NOD2 (40).

To explore the hypothesis that *Nod2* loss-of-function enhanced tumor responses during PD-1 immune checkpoint inhibition by causing intestinal dysbiosis, we performed quantitative metagenomic sequencing of colonic and rectal fecal pellets from $Nod2^{fs}$ and $Nod2^{wt}$ mice treated with anti-PD1 or untreated (*SI Appendix*, Fig. S7). Principal component analysis at the level of bacterial phyla (*SI Appendix*, Fig. S7*A*) or bacterial species (*SI Appendix*, Fig. S7*D*) separated stool samples from anti-PD1 treated mice from untreated mice but did not separate $Nod2^{fs}$ and $Nod2^{wt}$ mice. $Nod2^{fs}$ mice had greater diversity of bacterial phyla than $Nod2^{wt}$ mice measured by Shannon index at baseline (*SI Appendix*, Fig. S7*B*). Intriguingly, PD-1 blockade decreased bacterial diversity in $Nod2^{fs}$ mice but had little impact in $Nod2^{wt}$ mice (*SI Appendix*, Fig. S7*C*). Among the most abundant bacterial species, *Akkermansia muciniphila* and *Dubosiella newyorkiensis* were highest in untreated $Nod2^{fs}$ animals and reduced in anti-PD1 treated $Nod2^{fs}$ animals, whereas *Duncaniella sp001689575* and *sp001689425* became more abundant in $Nod2^{fs}$ animals posttreatment (*SI Appendix*, Fig. S7 *E* and *F*). Overall, these results indicate that the *Nod2* loss of function variants do not enhance tumor immune responses to PD1 blockade by causing large shifts in the population of intestinal bacteria, but do not rule out overgrowth of particular species.

Discussion

The goal of this study was to investigate the possibility that cancer immune response variability in people reflects, in part, inherited differences in immune tolerance checkpoints. The results above provide four complementary lines of evidence supporting that conclusion. NOD2 is known to play a critical "checkpoint" role, enabling the immune system to tolerate the large population of intestinal microbiota and avoid mounting the damaging inflammatory response responsible for Crohn's disease. In the results above, inherited loss-of-function *NOD2* variants were 1) biallelic in an exceptional case where local tumor irradiation triggered a systemic therapeutic response against metastatic melanoma and two different systemic autoimmune responses (Crohn's disease and vitiligo); 2) more frequently found in a large cohort of exceptional responder patients with lung cancer where pharmacological blockade of the PD-1 checkpoint promoted cancer survival and triggered an immune related adverse event; 3) more frequently found in patients with diverse cancers where pharmacological blockade of the PD-1 checkpoint triggered a therapeutic response against their cancer; and 4) experimentally increased the therapeutic response and CD8 effector T cell infiltration against a transplanted cancer in mice treated by pharmacological blockade of the PD-1 checkpoint.

In designing the prospective NSCLC clinical study, we made the a priori assumption that irAEs triggered by PD-1 blockade were suggestive of greater systemic immune activation and could be used to enrich for patients with germline predisposition to immunotherapy response. Since defining these criteria, retrospective analyses of NSCLC patients treated with anti-PD1/PDL1 have established a survival benefit for patients experiencing irAEs, with incremental benefit in patients with multiple or severe (grade 3 to 4) irAEs (3, 4, 42). In those studies it was unresolved whether greater immune activation reflected a more immunogenic tumor promoting paraneoplastic autoimmune reactions (43), differences in gut microbial flora (44–46), or inherited variability in immune response genes such as those in the major histocompatibility complex (47) or encoding Fc receptors for IgG (48). The results here do not exclude these other factors, but provide evidence that inherited defects in immune tolerance checkpoint genes are a common contributor.

Several seminal trials for single agent anti-PD-1/PD-L1 for NSCLC such as OAK (49) and POPLAR (50) have consent-based limitations on germline genome analyses, impacting available validation cohorts. Consent for WGS analysis has been performed for later trials that combined anti-PDL1 with chemotherapy within the IMpower suite [131/130/132/150 (51)], but analysis of these combination-treated cohorts showed no significant effect of *NOD2* genotype on clinical outcome. Speculatively, chemotherapy might perturb the intestinal barrier or augment cancer immunogenicity in other ways to obviate the beneficial effect of *NOD2* loss-of-function.

Downloaded from https://www.pnas.org by 138.25.168.236 on January 11, 2026 from IP address 138.25.168.236.

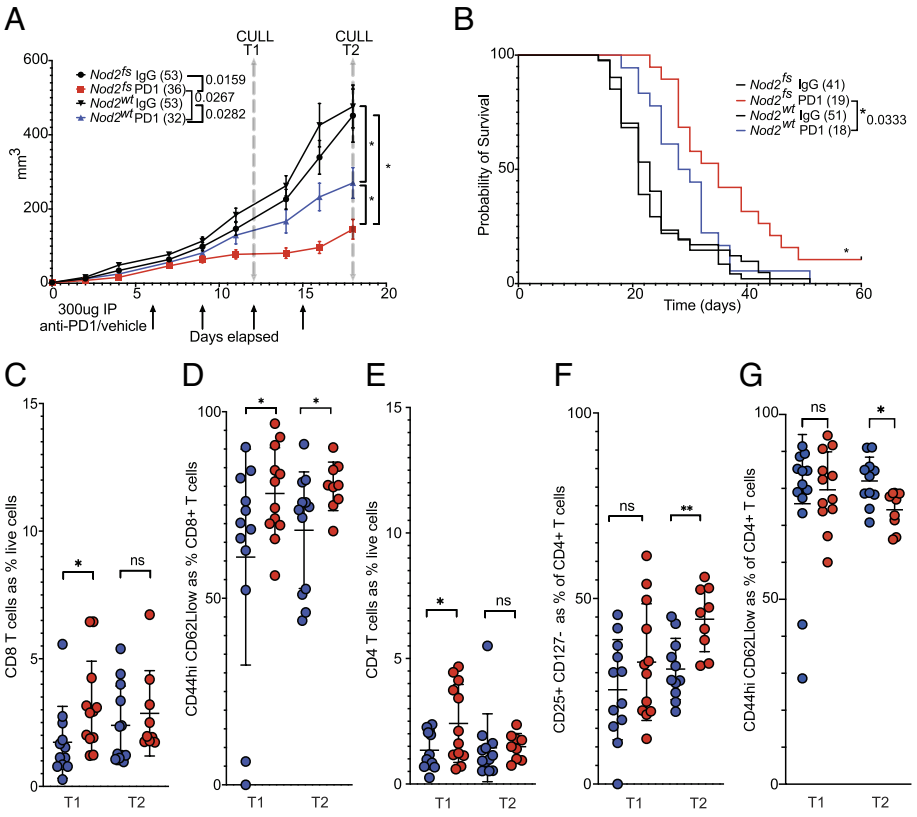

Fig. 5. Increased cancer immune responses elicited by anti-PD1 in mice with germline *NOD2* loss-of-function. *Nod2fs* or wildtype C57BL/6 mice were transplanted with MC38 cells subcutaneously in the flank and given four doses of anti-PD1 or control IgG. (*A*) Mean ± SEM tumor volume (n = 32-53 per group). (*B*) Kaplan–Meier survival curves (n = 18 to 42 per group). (*C*–*G*) Flow cytometric enumeration of tumor infiltrating cells in individual *Nod2fs* (red circles) or wildtype (blue circles) mice killed after two doses (T1) or four doses (T2) of anti-PD1. Bars denote mean and s.d. (*C*) CD8+ T cells as % of live cells in tumor. (*D*) CD44^{hi} CD62L^{low} cells as % of CD8+ T cells. (*E*) CD4+ T cells as % of live cells in tumor. (*F*) CD25+ CD127- cells as % of CD4+ T cells. (*G*) CD44^{hi} CD62L-^{low} cells as % of CD4+ T cells. Combined data from two replicate experiments; n = 15 to 18 per group. Growth curves compared by the Mann–Whitney test, survival curves compared by log-rank (Mantel-Cox) test. Flow cytometry analyses compared using the unpaired two-tailed *t* test. *$P < 0.05$; **$P < 0.01$; ns, not significant.

During manuscript revision we were able to access a public dataset of 202 exome sequences from NSCLC patients treated with single-agent anti-PD(L)1 (SU2C-MARK) (52). This cohort did not show a significant difference in survival outcomes according to *NOD2* LOF genotype, although information regarding irAEs was not available to identify the subset of patients who experienced irAEs. In our exceptional responders cohort and the INSPIRE cohort, where irAE data were available, NOD2 LOF was enriched in responders with an immune related adverse event but not in those without an irAE. Likewise, the exceptional responder melanoma patient with biallelic NOD2 LOF had multiple irAEs following stereotactic radiotherapy. This may indicate a requirement for *host predisposition* to breaking immune tolerance in order for inherited *NOD2* LOF to enhance the anticancer immune response.

Preexisting autoimmune disease was not associated with improved response to anti-PD1 in a large cohort of melanoma patients (53). By contrast, occurrence of irAEs during anti-PD1 treatment was strongly associated with improved OS in our NSCLC cohort, predicting a median OS of 48 mo. This is more than two-fold greater than irAE-selected survival in other cohorts, highlighting the unique enrichment for durable response alongside irAEs in this cohort (4, 42). *NOD2* LOF predicted survival in concert with psoriasis polygenic risk score but not nine other autoimmune disease polygenic risk scores. Psoriasis is driven by dysregulation of IL23/IL17 signaling and has significant mechanistic overlap with *NOD2*-associated inflammatory bowel disease despite minimal overlap of annotated risk SNPs (54–63), although in our cohort a lower polygenic risk for psoriasis and *NOD2* LOF was associated with better cancer survival. Other factors contributing predisposition to irAEs during cancer immunotherapy will be interesting to investigate in future studies.

In our prospectively recruited NSCLC cohort, higher than expected *NOD2* LOF alleles within 40 exceptional responders to anti-PD-1 was coupled with relative depletion of LOF alleles in 18 nonresponders. In the same cohort, a hyperactive allele of the NOD2 signal-transducing partner, *RIPK2*, was significantly enriched within nonresponders compared with exceptional responders and with the general population. Association of gain- and loss-of-function mutations with opposite clinical outcomes provides further evidence that less *NOD2* signaling is associated with heightened response to anti-PD1/PD-L1 monotherapy.

A difficult question for future studies is how does NOD2 function as an immune tolerance checkpoint, either in the context of Crohn's disease or immune reactions to cancer? In the context of the findings here, how does lower NOD2 signaling increase tumor infiltration with effector CD8 T cells and the therapeutic immune response to anti-PD-1? The role of NOD2 in sensing the large commensal population of gut bacteria seems likely to be significant, since germ free mice treated with anti-PD1 mount a poor immune response to MC38 tumor cells that is restored by a defined gut bacterial mixture, with the restored response dependent upon CD8 T cells (64).

Three distinct but not mutually exclusive hypothetical mechanisms may account for how the loss of NOD2 signaling paradoxically enhances immune responses, each involving commensal microbes. First, less NOD2 may cause intestinal dysbiosis or intestinal barrier deficits that increase exposure to microbial ligands for other innate sensors, thereby heightening immune stimulation (65). Alternatively, signaling by other innate immune sensors of bacteria may normally be dampened through feedback inhibitory pathways that are initiated by NOD2 signaling in response to chronic exposure either to MDP from diverse bacteria—a continuously produced pathogen-associated molecular pattern (PAMP) (17, 66)—or to sphingosine-1-phosphate produced by cells under metabolic stress as a continually produced stress-associated molecular pattern (SAMP) (67). In these PAMP or SAMP dampening hypotheses, less NOD2 signaling may release the response of other innate sensors from feedback inhibition to enhance immune stimulation.

There is varying evidence that *NOD2* loss-of-function causes dysbiosis (68–74). Our metagenomic analysis is consistent with Robertson et al. (70) and Goethel et al. (72) finding no discernable

Downloaded from https://www.pnas.org by 138.25.168.236 on January 11, 2026 from IP address 138.25.168.236.

difference in the composition of the stool in *Nod2*-deficient mice at the level of principal component analysis. This is also consistent with absence of substantial differences in stool microbiome in humans with NOD2 loss of function variants (74). Our study did not test for intestinal barrier deficits, which have been observed in *Nod2*-deficient mice to allow gut bacteria to reach lymph nodes or spleen (71, 75).

Metagenomic analysis of stool samples collected from patients with NSCLC or melanoma at baseline found increased microbial diversity in patients who subsequently responded to anti-PD1 (45, 46, 76). In one study, *Akkermansia muciniphila* was more abundant in stool samples from responding patients and correlated with increased Th1 reactivity as measured by IFNγ release (45). Consistent with these observations, the metagenomic analysis here found increased diversity and more abundant *Akkermansia muciniphila* in $Nod2^{fs}$ mice, who also make a better response when treated with anti-PD-1.

Feedback inhibition by chronic NOD2 signaling has been well documented in humans and mice. NOD2 is one of three pattern receptors recognizing bacterial cell wall peptidoglycans from diverse bacterial phyla, alongside NOD1 and TLR2. Each of these receptors recognizes a different peptidoglycan cleavage product, and they share the ability to activate NF-κB and other inflammatory transcription factors, albeit with markedly different qualities of response. The net immune effect of NOD2 stimulation is conditional on the duration of exposure to its ligand, MDP. Acute MDP exposure is proinflammatory and can enhance the response of other pattern recognition receptors. By contrast, chronic MDP exposure decreases the proinflammatory response not only to NOD2 restimulation, but to TLR2 and TLR4 stimulation. This inhibitory feedback on other microbial sensing pathways is abolished in monocyte-derived macrophages from mice or people who have inherited loss-of-function *NOD2* (17, 66). Chronic NOD2 engagement also cross-tolerizes receptors for endogenous danger signals that costimulate T cells, notably the NF-κB response to IL-1 (77). Increased exposure to MDP suppresses in vivo proliferation of ovalbumin-induced CD8 and CD4 T cells, acting through *NOD2* to induce GM-CSF and tolerogenic immature CD103+ dendritic cells (78). Extrapolating from these experimental results, our observation that tumor infiltrating CD8 effector T cells are increased in anti-PD1-treated NOD2 loss-of-function mice may reflect increased activation of mature dendritic cells, consistent with increased CD8+ dendritic cells in the tumors of $NOD2^{fs}$ mice observed at the T1 timepoint.

In the context of cancer immunity, manipulation of NOD2 signaling can give distinct outcomes based on the nature of intervention. A vaccine adjuvant stimulating NOD2 and TLR9 boosted CD8+ T cells and anticancer activity in mice (but not humans) when given as an intermittent bolus (two times weekly), simulating repetitive acute exposure (79, 80). Acute NOD2 stimulation also has the potential to act in synergy with anti-PD-L1. The effect of an *Enterococcus*-derived enzyme that enhanced anti-PD-L1 response in mice, SagA, was replicable using a NOD2-*active* isomer (but not a NOD2-*inactive* isomer) of MDP, a SagA cleavage product (81). Counter to this, NOD2 knockout mice mounted enhanced response to MCA-205 fibrosarcoma when treated with cyclophosphamide, an alkylating agent known to induce immunogenic cell death (75, 82). This was associated with a significant increase in accumulation of *Barnesiella* species in the colon and increased translocation of *Enterococcus hirae* to the spleen and lymph nodes. Both organisms had the capacity to increase CD8+ effector TILs when gavaged to antibiotic treated mice (75). In contrast to the cyclophosphamide treated mouse colony where *Barnesiella* accounted for 40 to 80% of colonic bacterial reads (75), this genus accounted for only 0.05% of metagenomic reads from the mice studied here and was not significantly different between anti-PD1 treated $Nod2^{fs}$ and $Nod2^{wt}$ mice.

The findings here indicate that less NOD2 signaling results in greater therapeutic response to cancer following immune stimulation in mice and humans. Regardless of mechanism, the results demonstrate that inherited variation in an innate immune sensor contributes to cancer immune response and that NOD2 is an important immune checkpoint not only for tolerating the gut microbiome but for tolerating cancer cells. Pharmacological inhibition of the NOD2 signaling pathway may represent a target for augmenting cancer immunotherapy and *NOD2/RIPK2* genotypes may serve as a predictive biomarker for anti-PD1 monotherapy in NSCLC.

Materials and Methods

Exceptional Responders Clinical Study Design and Recruitment. Patients were recruited from five tertiary hospitals across the Greater Sydney region who had been exposed to single agent anti-PD1/PDL1 for NSCLC between March 2012 to March 2020. Hospitals sites were Westmead Hospital, Blacktown Hospital, Chris O'Brien Lifehouse, Concord Repatriation General Hospital and St Vincent's Hospital Sydney. Eligible patients had stage IV NSCLC and were receiving, or were planned to receive treatment with single agent anti-PD-1/PD-L1. Patients had to be 18 y of age or older, willing to give a blood sample and able to give informed consent. Total patient numbers treated between March 2012 to March 2020 were generated from pharmacy dispensing records. Lists were filtered to identify those treated for NSCLC with single-agent anti-PD1/PDL1 using treating clinician (nonthoracic oncologists excluded), known treatment protocols, and analysis of medical records (final 742 patients). Total treatment pool was not calculated for the nationally recruiting program that provided the final 4 patients in the exceptional responder cohort. The data cut-off was June 25, 2020.

The principal researcher attended outpatient clinics over a 3-y period (between March 2017 and March 2020) under guidance of the treating clinicians, approaching patients for recruitment identified by the treating clinician. Alternatively, the treating clinician consented the patient. All patients approached (n = 144) were agreeable to participate in the study. Bloods were drawn at the time of consent and clinical data obtained retrospectively from the relevant electronic medical record. Human Research Ethics Committee (HREC) approval was granted for the overall project and Site-Specific Approvals gained for each participating site.

For inclusion in the nonresponder cohort, additional criteria beyond best response of progressive disease (per RECIST) were required to exclude patients with either 1) insufficient exposure to drug to elicit response (treatment duration of at least 2 mo or three doses) OR 2) atypical pathology/potential misdiagnoses distorting natural history of disease (overall survival ≤ 24 mo). Recruitment of such a patient group is inherently difficult because patients with shorter progression-free and overall survival are less likely to be captured during a set recruitment period. This is both because the patients attend clinic over a shorter period of time, and because unwell patients are less likely to attend outpatient appointments. Additionally, recruitment was purposefully targeted to exceptional responders–recruiting clinicians liaised with the PI to capture this population specifically. Incidental recruitment of nonresponders was thus low–with only 18 patients suitable for inclusion. Immune-related adverse events are less common in patients who gain no clinical benefit from checkpoint inhibitors compared with patients who do gain benefit (83). This is likely contributed to by shorter time on drug, less focus on (and documentation of) mild toxicities in unwell patients, and, significantly, the association between irAEs and improved outcomes in NSCLC treated with anti-PD-1/PD-L1 (3, 4, 84–88).

Whole Genome Sequencing. Patient genomes were sequenced on the Illumina HiSeq X platform using DNA extracted from whole blood (Qiagen, QIAamp DNA Mini Kit). Libraries were generated using the KAPA Hyper PCR-Free kit (Roche). Raw reads were aligned to the hs37d5 reference using BWA-MEM v0.7.10-r789, sorted and duplicate-marked with Novosort v1.03.01 (Novocraft Technologies). The GATK suite v3.3-0-g37228af was used for local indel realignment and base quality score recalibration (89). Genomic variant call formats (gVCFs) were generated with GATK HaplotypeCaller and variants recalibrated using GATK Variant Quality Score Recalibrator (VQSR). VCF files were annotated with Variant Effect Predictor (VEP) v79 using plugins including LoFTEE, dbNSFP v2.9, and CADD v1.3. Data were then assembled into GEMINI databases (v0.18.3). Finally, variants were imported into Seave (90).

Filtering Variants. Variant effect predictor (VEP)-annotated variant call files (vcf) generated from the Genome analysis Toolkit (GATK) pipeline were filtered for high

Downloaded from https://www.pnas.org by 138.25.168.236 on January 11, 2026 from IP address 138.25.168.236.

quality variants carried by individual patients (91). High quality variants were considered to have a filter flag of PASS, a variant quality of ≥ 120, a genotype quality > 40, a read depth >= 10, and for heterozygous variants the alternative allele required read support of at least 30% of total reads. All reported variants were manually inspected using the Integrative Genomics Viewer (IGV) to verify authenticity (www.broadinstitute.org/igv) using DNAnexus software (http://dnanexus.com).

dbGAP Cohort Analysis. Whole exome sequencing from nontumor samples for datasets with dbGAP accessions phs001565 (v1.c1 and v1.c3), phs000694, phs000980, phs001041, phs001075, phs002822, phs001940, and phs001618 were obtained in SRA format using prefetch from the SRA Toolkit (version 3.0.3) (92). The reads aligned to the *NOD2* region (chr 16, positions 50727517-50766986) were extracted in sam format with sam-dump from the same toolkit and converted to bam format using samtools (version 1.14) (93). Variants were then called using mpileup from bcftools (version 1.14) (93) with the final output being a variant call file (vcf) for each sample. The vcfs for all samples were merged using bcftools merge and variants at positions of interest were extracted with tabix from htslib (version 1.14) (94). Donor samples were annotated with metadata in R (version 4.2.2) (95) with RStudio (version 2022.12.0.353) (96) using data obtained from Miao et al. (97), Ravi et al. (52), and Anagnostou et al. (98). Data manipulations in R were performed with the tidyverse package (99). Metadata annotation included cancer type, treatment type, RECIST category, progression free survival (pfs), and overall survival (os). Donors were filtered to those who had received "anti-PD-1/anti-PD-L1" with pfs of more than 60 d before stratification by RECIST category and whether or not they carried germline loss of function *NOD2* variant(s) or the *RIPK2* GOF variant.

SNParray and Polygenic Risk Score Analysis. DNA was prepared from peripheral blood mononuclear cells with the QIAamp DSP DNA Blood Mini Kit according to the manufacturer's instructions, and analyzed on Thermo Fisher Axiom Precision Medicine Diversity arrays at the UNSW Ramaciotti Centre.

Array data were processed using command line Axiom Analysis Suite (version 2.11.6) by following the best practice workflow. Axiom call files were converted to plink and vcf formats using apt-format-result. Array data were quality controlled as described by Marees et al. (100). Two individuals were removed due to missing genotype data >0.02. Population stratification was performed using plink's (version v1.90b6.26) (101) MDS (dim = 10) using 1,000 genome data (release 20130502) as a reference population with thresholds for European ancestry set based on the first two components of the MDS. Beagle (version 5.4) was used to phase genotypes (102) and impute nongenotyped markers (103) using phased 1,000 genome project data as a reference (release 20181203).

To calculate polygenic risk, variant call files were submitted to Michigan Imputation Server's Polygenic Score Calculation (104) using 1000G Phase 1 v3 Shapeit2 as a reference panel and PGS Catalog (pgs-catalog-20231101) for polygenic risk scoring (105).

PRSs for autoimmune diseases were imported into R before integrating the NOD2 genotype information and patient metadata such as overall survival and RECIST score. Kaplan–Meier plots were generated in R using the ggsurvfit package and were censored by death. Survival curve differences were tested using the log-rank test as implemented by the survdiff function with weighting for death events.

Producing NOD2-Deficient Mice. *Nod2*^{fs} mice were produced by the Mouse Engineering Garvan/ABR (MEGA) Facility (Moss Vale and Sydney, Australia) by CRISPR/*Cas9* gene targeting in C57BL/6 J mouse embryos following established molecular and animal husbandry techniques (106). A single guide RNA was designed to target within Exon 3 (target with protospacer-associated motif underlined = GCTTGATCTCGCTGCGGTGAAGG) and coinjected with polyadenylated *Cas9* mRNA into C57BL/6 J zygotes. Microinjected embryos were cultured overnight and introduced into pseudopregnant foster mothers. Pups were screened by PCR and Sanger sequencing of ear-punch DNA and a founder mouse identified that carried a 289 bp microhomology-mediated deletion that removed the 3′ 88 bp of Exon 3 and the associated splice donor sequences (*SI Appendix*, Fig. S3). The targeted allele was maintained by breeding on a C57BL/6 J background. C57BL/6 J control animals were purchased from the Australian BioResources (Moss Vale, New South Wales). *Nod2*^{fs} mice had no overt phenotype, and no discernable differences in lymphocyte subsets at baseline, in response to immunization with sheep red blood cells, or in aged mice (37 to 49 wk) compared with *Nod2*^{wt} animals.

Cell Lines and Tissue Culture. MC38 mouse colon adenocarcinoma cells were kindly provided by the Michele Teng laboratory, QIMR Berghofer. Early passage cancer cells were cultured within TC-treated flasks (Corning cell culture) at 37 °C in DMEM supplemented with 10% FCS, 100 IU/mL penicillin, 100 μg/mL streptomycin, 2 mM L-glutamine, and 100 μM NEAA, sodium pyruvate, and HEPES. Cells were dissociated using 1.5 (T75) to 3 mL (T150) of trypsin/EDTA and passaged for expansion at a 1:20 dilution.

In Vivo Mouse Studies. Age- and sex-matched C57BL/6 *Nod2*^{fs} or *Nod2*^{wt} mice were inoculated with 1 × 10^6 MC38 cells subcutaneously on the left flank. For vehicle-control experiments, mice were grouped based on tumor size and treated by intraperitoneal injection with 300 μg of the rat IgG2a monoclonal antibody RMP1-14 against mouse PD-1, which blocks PD-1 binding to PDL1 and PDL2 (107) or rat IgG2a isotype control, anti-trinitrophenol (both obtained from BioXCell) every third day for four doses. For subsequent experiments, all animals received anti-PD1 treatment that was commenced between days 5 to 7, when >75% of tumors were palpable. Perpendicular tumor diameters were measured 2nd daily using digital calipers, area was calculated using the formula LxW, where L is the longest dimension (mm^2).

Mice were culled using carbon dioxide (CO_2) asphyxiation prior to experimental endpoints if any of the following ethical endpoints were met: weight loss ≥20% compared to maximum body weight OR overnight weight loss of ≥10%, tumor mass ≥10% of body weight, tumor ulceration >2 mm, tumor interferes with mobility and affects access to food and water, body condition score of ≤2 (where body condition (BC) of 1 is emaciated, BC5 is obese and BC3 is well conditioned), presence of one of more signs of distress: eyelids partially closed, rough coat, respiration changes, unusual posturing, or behavior. All experiments were approved by the Garvan Animal Ethics Committee.

Bone Marrow Derived Macrophages: Culture and Stimulation. After the mice were killed by CO_2 asphyxiation, femurs and tibiae were dissected and marrow was flushed by passing sterile PBS through a syringe and 23 g needle, filtered, lysed, rinsed, and resuspended. Cells were plated at 2 × 10^6 per 10 cm bacterial dish in 7 mL of 10% FBS RPMI supplemented with Pen/Strep, D-glucose (final concentration: 4.5 g/L); and Glutamax (stable glutamine, Gibco) with 50 ng/mL M-CSF (Sino Biological), cultured for 6 d at 37 °C and harvested using PBS and a cell scraper. Macrophages from the cultures above were seeded as 2 × 10^5 cells/well in 200μL of the same medium, without M-CSF. After 30 min, 10 μg/mL MDP (Invivogen) was added and incubated at 37 °C for 24 h, LPS (Invivogen) was added to relevant wells (200 ng/mL) for the final 3 h. Cells were transferred to ice after elapsed time and ELISA performed on conditioned medium.

ELISA. Cytokine levels for IL8/KC were quantified by ELISA according to the manufacturer's instructions (DuoSet ELISA kit, R&D Systems).

Flow Cytometry. On the day of harvest, spleen and tumor were collected into PBS with 1% BSA. Tumors were manually divided and then digested over 60 min using collagenase enzyme 10 mg/mL in RPMI supplemented with 10 mM HEPES and 2.5% FBS at 37 °C.

Cell suspensions were passed through a 70 μm cell strainer (Falcon, Corning, NY) and centrifuged at 1,500 rpm (440 g) for 5 minu at 4 °C. Fc receptors were blocked with unlabeled anti-CD16/32 (ebioscience) before staining.

Tumor and spleen cells were counted and resuspended in PBS before plating 2 × 10^6 cells/well in 96-well plates (Thermo Fisher Scientific). Tumor and spleen cells were stained with the following, given in format - Antibody fluorophore (Company, clone):

CD127 FITC (BioLegend, A7R34), CD11c PerCP Cy5.5 (e-Bioscience, N418), CD11b APC (BD Biosciences, M1/70), CD25 APC Cy7 (BioLegend, PC61), CD44 PE (BD Pharmingen, IM7), Ly6c biotin (BioLegend, HK1.4), F4/80 BV421 (BioLegend, BM8), CD62L BV605 (BioLegend, MEL-14), Ly6G BV711 (BioLegend, 1A8), CD4 BV786 (BD Biosciences, GK1.5), CD8 BUV395 (BD Biosciences, RPA-T8), and B220 BUV737 (BD Pharmingen, RA3-6B2). Zombie aqua (BioLegend) was used for all cells.

Cells were filtered using 70 μm filter round-bottom FACS tubes (BD Pharmingen) immediately before data acquisition on a LSR II analyzer (BD Pharmingen). Cytometer files were analyzed with FlowJo software (FlowJo LLC, Ashland, OR).

Mouse Gut Microbiome Metagenomic Analysis. Mice received 4 IP doses of 300 μg anti-PD1 or vehicle over 2 wk, were killed., and feces were collected from the terminal colon or rectum and snap frozen in liquid nitrogen. Total DNA was extracted from mouse stool samples using the QIAamp DNA mini Kit (Qiagen, #51304) as per the manufacturer's instructions, with the addition of a physical

Downloaded from https://www.pnas.org by 138.25.168.236 on January 11, 2026 from IP address 138.25.168.236.

lysis step following incubation in lysis buffer. DNA was eluted, and concentration measured with Qubit dsDNA HS Assay Kit (Life Technologies, #Q32853) and Qubit Fluorometer (Life Technologies). Purified DNA was aliquoted for downstream applications and stored at−80 °C. For shotgun metagenomic sequencing, library preparation was performed with Nextera DNA Flex Library Prep (#20018705) for Nextera DNA CD Indexes (Illumina, #20018708) as per the manufacturer's instructions. Libraries were sequenced on a NovaSeq 6000 Sequencing System (Illumina, #20012850) at the Ramaciotti Centre for Genomics (UNSW Sydney).

Deduplication of the metagenomic reads was carried out using BBmap/clumpify.sh (version 38.90) 1). Next, using minimap2 (version 2.18) 2), sequencing reads were mapped against the human genome (hg38), and the mapped reads were removed. The low-quality metagenomic reads were then processed with fastp (version 0.20.1) 3). Compositional profiling was performed by Kraken2 (version 2.1.1) 4) with the Genome Taxonomy Database (GTDB) 5).

Statistical analysis was completed in R (v4.2.1). Alpha diversities were estimated at the species level and then differences across groups were identified using Kruskal–Wallis with Dunn's post hoc test. The differences in the bacterial community were shown using the Principal Component Analysis, and the significance of variance was tested using the Permutational multivariate ANOVA with permutation of 999. The Kruskal–Wallis with Dunn's post hoc test were performed to identify the microbial features that varied substantially between groups. Using the Benjamini–Hochberg multiple test correction, all *P* values were adjusted. *P* values of <0.05 were considered statistically significant.

Statistical Analysis. For clinical studies, progression-free survival and overall survival were calculated from date of anti-PD-1/PD-L1 commencement to date of radiological progression or death, or date of death respectively. Tumor response was investigator-assessed according to the Response Evaluation Criteria in Solid Tumors, version 1.1 (108).

For preclinical studies, GraphPad Prism 6 (GraphPad Software, San Diego, USA) was used for data analysis. For all tests $P < 0.05$ was considered as being statistically significant. For all data presented, $*P < 0.05$, $**P < 0.01$, $***P < 0.001$, $****P < 0.0001$.

Data, Materials, and Software Availability. All study data are included in the article and/or *SI Appendix*.

ACKNOWLEDGMENTS. All patients involved in this study were remarkably generous with their time, bodies, and medical information, for no personal benefit. We thank all those involved and their families. MC38 cell line kindly provided by Associate Professor Michele Teng, Cancer Immunoregulation and Immunotherapy Laboratory at the Queensland Institute of Medical Research Berghofer Institute. Assistance with design, approval, and implementation of a clinical trial protocol was provided by Dr. Mandy Ballinger, Genetic Cancer Risk Group, Garvan Institute of Medical Research. Assistance with a statistical approach for the clinical study was provided by Professor Greg Gibson, Center for Integrative Genomics, Georgia Tech School of Biological Sciences. Professor Martin Henry Norman Tattersall (deceased) was an instrumental advocate of the project and mentor of M. Barnet. Several of Professor Tattersall's former patients were included in the analysis. Portions of this work were originally part of the PhD thesis of coauthor M.B.B. M.B.B. was supported by scholarships from the University of NSW Sydney, Australian Genomics Health Alliance and Sydney Catalyst, and fellowships from The Beverley Alt Foundation and Lindy and Avrom Sank. A.B. was supported by a fellowship from the Department of Health and Human Services acting through the Victorian Cancer Agency. I.D.D. was supported in part by a National Health and Medical Research Council Investigator Grant (2016274). This work was supported by the Bill and Patricia Ritchie Foundation Chair in Immunogenomics and by funding for the Exceptional Responders Program from Bioplatforms Australia and The Kinghorn Foundation.

Author affiliations: [a]Immunology Division, Garvan Institute of Medical Research, Darlinghurst, NSW 2010, Australia; [b]St Vincent's Clinical School, University of New South Wales Sydney, Kensington, NSW 2052, Australia; [c]Department of Medical Oncology, The Kinghorn Cancer Centre, St Vincent's Hospital Sydney, Darlinghurst, NSW 2010, Australia; [d]School of Biomedical Engineering, University of Technology Sydney, Ultimo, NSW 2007, Australia; [e]Cellular Genomics Futures Institute & School of Biomedical Sciences, University of New South Wales Sydney, Kensington, NSW 2052, Australia; [f]School of Medicine, Monash University, Clayton, VIC 3800, Australia; [g]Olivia Newton-John Cancer Research Institute, Heidelberg, VIC 3084, Australia; [h]Eastern Health Clinical School, Eastern Health, Box Hill, VIC 3128, Australia; [i]National Health and Medical Research Council Clinical Trials Centre, University of Sydney, Camperdown, NSW 2050, Australia; [j]Genentech, South San Francisco, CA 94080-4990; [k]Princess Margaret Cancer Centre, Toronto, ON M5G 2M9, Canada; [l]School of Cancer Medicine, La Trobe University, Heidelberg, VIC 3084, Australia; [m]School of Medicine, University of Melbourne, Parkville, VIC 3010, Australia; [n]UNSW Microbiome Research Centre, University of New South Wales Sydney, Kogarah, NSW 2217, Australia; [o]School of Medicine, Western Sydney University, Penrith, NSW 2751, Australia; [p]Sydney Medical School, University of Sydney, Camperdown, NSW 2050, Australia; [q]Department of Tissue Pathology and Diagnostic Oncology, NSW Health Pathology, Royal Prince Alfred Hospital, Camperdown, NSW 2050, Australia; [r]Blacktown Cancer and Haematology Centre, Blacktown Mount Druitt Hospital, Blacktown, NSW 2148, Australia; [s]Crown Princess Mary Cancer Centre, Westmead Hospital, Westmead, NSW 2145, Australia; [t]Peter MacCallum Cancer Centre, Melbourne, VIC 3000, Australia; [u]Canberra Region Cancer Centre, Garran, ACT 2605, Australia; [v]School of Clinical Medicine, Hong Kong University Health System, Hong Kong; [w]Chris O'Brien Lifehouse, Camperdown, NSW 2050, Australia; and [x]Concord Cancer Centre, Concord Repatriation General Hospital, Concord, NSW 2138, Australia

Author contributions: M.B.B., K.J.L.J., R.B., Z.K., J.B., G.L.H., F.Z., W.A.C., A.M.J., P.L.B., S.C.K., J.C., and C.C.G. designed research; M.B.B., K.J.L.J., E.M.-F., A.R., D.L.B., A.C., C.J.J., M.F., A.M., T.J.P., K.W., I.A., S.J., I.D.D., G.H., Z.K., J.B., C.Y., S.P., T.P., A.B., G.L.H., F.Z., W.A.C., B.G., A.N., A.M.J., T.J., G.P., R.H., M.B., P.L.B., S.C.K., and J.C. performed research; R.B. contributed new reagents/analytic tools; M.B.B., K.J.L.J., E.M.-F., A.R., D.L.B., C.J.J., M.F., T.J.P., R.B., S.J., I.D.D., G.H., Z.K., J.B., C.Y., S.P., T.P., A.B., G.L.H., F.Z., W.A.C., B.G., A.N., A.M.J., T.J., G.P., R.H., M.B., P.L.B., S.C.K., J.C., and C.C.G. analyzed data; and M.B.B., K.J.L.J., J.C., and C.C.G. wrote the paper.

1. C. C. Goodnow *et al.*, Self-tolerance checkpoints in B lymphocyte development. *Adv. Immunol.* **59**, 279–368 (1995).
2. A. J. Korman, K. S. Peggs, J. P. Allison, Checkpoint blockade in cancer immunotherapy. *Adv. Immunol.* **90**, 297–339 (2006).
3. D. Maillet *et al.*, Association between immune-related adverse events and long-term survival outcomes in patients treated with immune checkpoint inhibitors. *Eur. J. Cancer* **132**, 61–70 (2020).
4. B. Ricciuti *et al.*, Impact of immune-related adverse events on survival in patients with advanced non-small cell lung cancer treated with nivolumab: Long-term outcomes from a multi-institutional analysis. *J. Cancer Res. Clin. Oncol.* **145**, 479–485 (2019).
5. H. Nishimura, M. Nose, H. Hiai, N. Minato, T. Honjo, Development of lupus-like autoimmune diseases by disruption of the PD-1 gene encoding an ITIM motif-carrying immunoreceptor. *Immunity* **11**, 141–151 (1999).
6. C. E. Teh, S. R. Daley, A. Enders, C. C. Goodnow, T-cell regulation by casitas B-lineage lymphoma (Cblb) is a critical failsafe against autoimmune disease due to autoimmune regulator (Aire) deficiency. *Proc. Natl. Acad. Sci. U. S. A.* **107**, 14709–14714 (2010).
7. R. J. Cornall *et al.*, Polygenic autoimmune traits: Lyn, CD22, and SHP-1 are limiting elements of a biochemical pathway regulating BCR signaling and selection. *Immunity* **8**, 497–508 (1998).
8. R. J. Bramhall, K. Mahady, A. H. Peach, Spontaneous regression of metastatic melanoma – Clinical evidence of the abscopal effect. *Eur. J. Surg. Oncol.* **40**, 34–41 (2014).
9. D. K. Bonen *et al.*, Crohn's disease-associated NOD2 variants share a signaling defect in response to lipopolysaccharide and peptidoglycan. *Gastroenterology* **124**, 140–146 (2003).
10. N. Inohara *et al.*, Host recognition of bacterial muramyl dipeptide mediated through NOD2. Implications for Crohn's disease. *J. Biol. Chem.* **278**, 5509–5512 (2003).
11. M. Economou, T. A. Trikalinos, K. T. Loizou, E. V. Tsianos, J. P. Ioannidis, Differential effects of NOD2 variants on Crohn's disease risk and phenotype in diverse populations: a metaanalysis. *Am. J. Gastroenterol.* **99**, 2393–2404 (2004).
12. Y. Ogura *et al.*, A frameshift mutation in NOD2 associated with susceptibility to Crohn's disease. *Nature* **411**, 603–606 (2001).
13. J. Hampe *et al.*, Association between insertion mutation in NOD2 gene and Crohn's disease in German and British populations. *Lancet* **357**, 1925–1928 (2001).
14. R. Parkhouse, T. P. Monie, Dysfunctional crohn's disease-associated NOD2 Polymorphisms cannot be reliably predicted on the basis of RIPK2 binding or membrane association. *Front. Immunol.* **6**, 521 (2015).
15. P. Lacaze *et al.*, The medical genome reference bank: A whole-genome data resource of 4000 healthy elderly individuals. Rationale and cohort design. *Eur. J. Hum. Genet.* **27**, 308–316 (2019).
16. V. Souvannavong, A. Adam, Opposite effects of the synthetic adjuvant N-acetyl-muramyl-L-alanyl-D-isoglutamine on the immune response in mice depending on experimental conditions. *Eur. J. Immunol.* **10**, 654–656 (1980).
17. M. Hedl, J. Li, J. H. Cho, C. Abraham, Chronic stimulation of Nod2 mediates tolerance to bacterial products. *Proc. Natl. Acad. Sci. U.S.A.* **104**, 19440-19445 (2007).
18. Z. Zídek, J. Capková, M. Boubelík, K. Masek, Opposite effects of the synthetic immunomodulator, muramyl dipeptide, on rejection of mouse skin allografts. *Eur. J. Immunol.* **13**, 859–861 (1983).
19. L. Horn *et al.*, Nivolumab versus docetaxel in previously treated patients with advanced non-small-cell lung cancer: Two-year outcomes from two randomized, open-label, phase III trials (CheckMate 017 and CheckMate 057). *J. Clin. Oncol.* **35**, 3924–3933 (2017).
20. J. Schachter *et al.*, Pembrolizumab versus ipilimumab for advanced melanoma: Final overall survival results of a multicentre, randomised, open-label phase 3 study (KEYNOTE-006). *Lancet* **390**, 1853–1862 (2017).
21. R. S. Herbst *et al.*, Pembrolizumab versus docetaxel for previously treated, PD-L1-positive, advanced non-small-cell lung cancer (KEYNOTE-010): A randomised controlled trial. *Lancet* **387**, 1540–1550 (2016).
22. Anonymous Pharmaceutical Benefits Scheme, *Recommendations made by the PBAC* (Department of Health, Canberra, 2019).
23. E. E. Vokes *et al.*, Nivolumab versus docetaxel in previously treated advanced non-small-cell lung cancer (CheckMate 017 and CheckMate 057): 3-year update and outcomes in patients with liver metastases. *Ann. Oncol.* **29**, 959–965 (2018).
24. M. Chamaillard *et al.*, Gene-environment interaction modulated by allelic heterogeneity in inflammatory diseases. *Proc. Natl. Acad. Sci. U. S. A.* **100**, 3455–3460 (2003).
25. T. Tanabe *et al.*, Regulatory regions and critical residues of NOD2 involved in muramyl dipeptide recognition. *EMBO J.* **23**, 1587–1597 (2004).
26. M. A. Rivas *et al.*, Deep resequencing of GWAS loci identifies independent rare variants associated with inflammatory bowel disease. *Nat. Genet.* **43**, 1066–1073 (2011).

Downloaded from https://www.pnas.org by 138.25.168.236 on January 11, 2026 from IP address 138.25.168.236.

27. K. J. Karczewski *et al.*, The mutational constraint spectrum quantified from variation in 141, 456 humans. *Nature* **581**, 434–443 (2020).
28. S. Lesage *et al.*, *CARD15/NOD2* mutational analysis and genotype-phenotype correlation in 612 patients with inflammatory bowel disease. *Am. J. Hum. Genet.* **70**, 845–857 (2002).
29. R. Arthur, O. Schulz-Trieglaff, A. J. Cox, J. O'Connell, AKT: Ancestry and kinship toolkit. *Bioinformatics* **33**, 142–144 (2016).
30. C. A. Stafford *et al.*, Phosphorylation of muramyl peptides by NAGK is required for NOD2 activation. *Nature* **609**, 590–596 (2022).
31. T. Goncharov *et al.*, Disruption of XIAP–RIP2 Association Blocks NOD2-Mediated Inflammatory Signaling. *Mol. Cell* **69**, 551–565.e557 (2018).
32. C. Speckmann *et al.*, X-linked inhibitor of apoptosis (XIAP) deficiency: The spectrum of presenting manifestations beyond hemophagocytic lymphohistiocytosis. *Clin. Immunol.* **149**, 133–141 (2013).
33. M. Takeuchi *et al.*, Dense genotyping of immune-related loci implicates host responses to microbial exposure in Behçet's disease susceptibility. *Nat. Genet.* **49**, 438–443 (2017).
34. M. J. Jurynec *et al.*, A hyperactivating proinflammatory RIPK2 allele associated with early-onset osteoarthritis. *Hum. Mol. Genet.* **27**, 2383–2391 (2018).
35. S. Y. Cindy Yang *et al.*, Pan-cancer analysis of longitudinal metastatic tumors reveals genomic alterations and immune landscape dynamics associated with pembrolizumab sensitivity. *Nat. Commun.* **12**, 5137 (2021).
36. T. H. Corbett, D. P. Griswold Jr., B. J. Roberts, J. C. Peckham, F. M. Schabel Jr., Tumor induction relationships in development of transplantable cancers of the colon in mice for chemotherapy assays, with a note on carcinogen structure. *Cancer Res.* **35**, 2434–2439 (1975).
37. S. F. Ngiow *et al.*, Anti-TIM3 antibody promotes T cell IFN-γ-mediated antitumor immunity and suppresses established tumors. *Cancer Res.* **71**, 3540–3551 (2011).
38. S. F. Ngiow *et al.*, A threshold level of intratumor CD8+ T-cell PD1 expression dictates therapeutic response to anti-PD1. *Cancer Res.* **75**, 3800–3811 (2015).
39. B. Wang, *et al.*, Combination cancer immunotherapy targeting PD-1 and GITR can rescue CD8(+) T cell dysfunction and maintain memory phenotype *Sci. Immunol.* **3**, eaat7061 (2018), 10.1126/sciimmunol.aat7061.
40. M. Yadav *et al.*, Predicting immunogenic tumour mutations by combining mass spectrometry and exome sequencing. *Nature* **515**, 572–576 (2014).
41. M. Efremova *et al.*, Targeting immune checkpoints potentiates immunoediting and changes the dynamics of tumor evolution. *Nat. Commun.* **9**, 32 (2018).
42. S. Cook, *et al.*, Immune-related adverse events and survival among patients with metastatic NSCLC treated with immune checkpoint inhibitors *JAMA Netw. Open.* **7**, e2352302 (2024) 10.1001/jamanetworkopen.2023.52302.
43. N. McGranahan *et al.*, Clonal neoantigens elicit T cell immunoreactivity and sensitivity to immune checkpoint blockade. *Science* **351**, 1463–1469 (2016).
44. V. Matson *et al.*, The commensal microbiome is associated with anti-PD-1 efficacy in metastatic melanoma patients. *Science* **359**, 104–108 (2018).
45. B. Routy *et al.*, Gut microbiome influences efficacy of PD-1-based immunotherapy against epithelial tumors. *Science* **359**, 91–97 (2018).
46. V. Gopalakrishnan *et al.*, Gut microbiome modulates response to anti-PD-1 immunotherapy in melanoma patients. *Science* **359**, 97–103 (2018).
47. D. Chowell *et al.*, Patient HLA class I genotype influences cancer response to checkpoint blockade immunotherapy. *Science* **359**, 582–587 (2018).
48. P. Smith, D. J. DiLillo, S. Bournazos, F. Li, J. V. Ravetch, Mouse model recapitulating human Fcγ receptor structural and functional diversity. *Proc. Natl. Acad. Sci. U. S. A.* **109**, 6181–6186 (2012).
49. A. Rittmeyer *et al.*, Atezolizumab versus docetaxel in patients with previously treated non-small-cell lung cancer (OAK): A phase 3, open-label, multicentre randomised controlled trial. *Lancet* **389**, 255–265 (2017).
50. L. Fehrenbacher *et al.*, Atezolizumab versus docetaxel for patients with previously treated non-small-cell lung cancer (POPLAR): A multicentre, open-label, phase 2 randomised controlled trial. *Lancet* **387**, 1837–1846 (2016).
51. Z. Khan *et al.*, Genetic variation associated with thyroid autoimmunity shapes the systemic immune response to PD-1 checkpoint blockade. *Nat. Commun.* **12**, 3355 (2021).
52. A. Ravi *et al.*, Genomic and transcriptomic analysis of checkpoint blockade response in advanced non-small cell lung cancer. *Nat. Genet.* **55**, 807–819 (2023).
53. M. K. van der Kooij *et al.*, Safety and efficacy of checkpoint inhibition in patients with melanoma and preexisting autoimmune disease: A cohort study. *Ann. Intern. Med.* **174**, 641–648 (2021).
54. Y. Fu, C. H. Lee, C. C. Chi, Association of psoriasis with inflammatory bowel disease: A systematic review and meta-analysis. *JAMA Dermatol.* **154**, 1417–1423 (2018).
55. R. Hoffmann, G. Schieferstein, F. Schunter, H. Jenss, Re: Increased occurrence of psoriasis in patients with Crohn's disease and their relatives. *Am. J. Gastroenterol.* **86**, 787–788 (1991).
56. S. A. Lambert *et al.*, Enhancing the Polygenic Score Catalog with tools for score calculation and ancestry normalization. *Nat Genet.* **56**, 1989–1994 (2024).
57. A. E. Wight, *et al.*, Antibody-mediated blockade of the IL23 receptor destabilizes intratumoral regulatory T cells and enhances immunotherapy *Proc. Natl. Acad. Sci. U. S. A.* **119**, e2200757119 (2022), 10.1073/pnas.2200757119.
58. J. L. Langowski *et al.*, IL-23 promotes tumour incidence and growth. *Nature* **442**, 461–465 (2006).
59. L. Puig *et al.*, The biological basis of disease recurrence in psoriasis: A historical perspective and current models. *Br. J. Dermatol.* **186**, 773–781 (2022).
60. C. Schinocca, *et al.*, Role of the IL-23/IL-17 pathway in rheumatic diseases: An overview *Front. Immunol.* **12**, 637829 (2021), 10.3389/fimmu.2021.637829.
61. C. Liu, *et al.*, Blocking IL-17A enhances tumor response to anti-PD-1 immunotherapy in microsatellite stable colorectal cancer *J. Immunother. Cancer* **9**, e001895 (2021) 10.1136/jitc-2020-001895.
62. R. Váraljai *et al.*, Interleukin 17 signaling supports clinical benefit of dual CTLA-4 and PD-1 checkpoint inhibition in melanoma. *Nat. Cancer* **4**, 1292–1308 (2023).
63. P. Miossec, J. K. Kolls, Targeting IL-17 and TH17 cells in chronic inflammation. *Nat. Rev. Drug. Discov.* **11**, 763–776 (2012).
64. T. Tanoue *et al.*, A defined commensal consortium elicits CD8 T cells and anti-cancer immunity. *Nature* **565**, 600–605 (2019).
65. D. Knights, K. G. Lassen, R. J. Xavier, Advances in inflammatory bowel disease pathogenesis: Linking host genetics and the microbiome. *Gut* **62**, 1505–1510 (2013).
66. T. Watanabe, A. Kitani, P. J. Murray, W. Strober, NOD2 is a negative regulator of Toll-like receptor 2–mediated T helper type 1 responses. *Nat. Immunol.* **5**, 800–808 (2004).
67. G. Pei, *et al.*, Cellular stress promotes NOD1/2-dependent inflammation via the endogenous metabolite sphingosine-1-phosphate *EMBO J.* **40**, e106272 (2021), 10.15252/embj.2020106272.
68. S. Mondot *et al.*, Altered gut microbiota composition in immune-impaired Nod2(-/-) mice. *Gut* **61**, 634–635 (2012).
69. A. Rehman *et al.*, Nod2 is essential for temporal development of intestinal microbial communities. *Gut* **60**, 1354–1362 (2011).
70. S. J. Robertson *et al.*, Nod1 and Nod2 signaling does not alter the composition of intestinal bacterial communities at homeostasis. *Gut. Microbes* **4**, 222–231 (2013).
71. T. Petnicki-Ocwieja *et al.*, Nod2 is required for the regulation of commensal microbiota in the intestine. *Proc. Natl. Acad. Sci. U.S.A.* **106**, 15813–15818 (2009).
72. A. Goethel *et al.*, Nod2 influences microbial resilience and susceptibility to colitis following antibiotic exposure. *Mucosal Immunol.* **12**, 720–732 (2019).
73. D. Carlos *et al.*, NOD2 deficiency promotes intestinal CD4+ T lymphocyte imbalance, metainflammation, and aggravates type 2 diabetes in murine model. *Front. Immunol.* **11**, 1265 (2020).
74. N. A. Kennedy *et al.*, The impact of NOD2 variants on fecal microbiota in Crohn's disease and controls without gastrointestinal disease. *Inflamm. Bowel Dis.* **24**, 583–592 (2018).
75. R. Daillère *et al.*, *Enterococcus hirae* and *Barnesiella intestinihominis* facilitate cyclophosphamide-induced therapeutic immunomodulatory effects. *Immunity* **45**, 931–943 (2016).
76. R. C. Newsome *et al.*, Interaction of bacterial genera associated with therapeutic response to immune checkpoint PD-1 blockade in a United States cohort. *Genome Med.* **14**, 35 (2022).
77. M. Hedl, C. Abraham, Secretory mediators regulate Nod2-induced tolerance in human macrophages. *Gastroenterology* **140**, 231–241 (2011).
78. D. Prescott *et al.*, NOD2 modulates immune tolerance via the GM-CSF-dependent generation of CD103(+) dendritic cells. *Proc. Natl. Acad. Sci. U. S. A.* **117**, 10946–10957 (2020).
79. M. Ishihara *et al.*, First-in-human phase I clinical trial of the NY-ESO-1 protein cancer vaccine with NOD2 and TLR9 stimulants in patients with NY-ESO-1-expressing refractory solid tumors. *Cancer Immunol. Immunother.* **69**, 663–675 (2020).
80. R. C. Girvan *et al.*, MIS416, a non-toxic microparticle adjuvant derived from Propionibacterium acnes comprising immunostimulatory muramyl dipeptide and bacterial DNA promotes cross-priming and Th1 immunity. *Vaccine* **29**, 545–557 (2011).
81. M. E. Griffin *et al.*, *Enterococcus* peptidoglycan remodeling promotes checkpoint inhibitor cancer immunotherapy. *Science* **373**, 1040–1046 (2021).
82. O. Kepp, *et al.*, Consensus guidelines for the detection of immunogenic cell death *Oncoimmunology* **3**, e955691 (2014), 10.4161/21624011.2014.955691.
83. V. E. Maher *et al.*, Analysis of the association between adverse events and outcome in patients receiving a programmed death protein 1 or programmed death ligand 1 antibody. *J. Clin. Oncol.* **37**, 2730–2737 (2019).
84. K. Haratani *et al.*, Association of immune-related adverse events with nivolumab efficacy in non-small-cell lung cancer. *JAMA Oncol.* **4**, 374–378 (2018).
85. M. Riudavets *et al.*, Correlation between immune-related adverse events (irAEs) and efficacy in patients with solid tumors treated with immune-checkpoints inhibitors (ICIs). *J. Clin. Oncol.* **36**, 3064–3064 (2018).
86. J. Rogado *et al.*, Immune-related adverse events predict the therapeutic efficacy of anti-PD-1 antibodies in cancer patients. *Eur. J. Cancer* **109**, 21–27 (2019).
87. H. Akamatsu, *et al.*, Immune-related adverse events by immune checkpoint inhibitors significantly predict durable efficacy even in responders with advanced non-small cell lung cancer. *Oncologist* **25**, e679 –e683 (2020).
88. S. L. Topalian *et al.*, Five-year survival and correlates among patients with advanced melanoma, renal cell carcinoma, or non-small cell lung cancer treated with nivolumab. *JAMA Oncol.* **5**, 1411–1420 (2019).
89. A. McKenna *et al.*, The genome analysis toolkit: A MapReduce framework for analyzing next-generation DNA sequencing data. *Genome Res.* **20**, 1297–1303 (2010).
90. V. Gayevskiy, T. Roscioli, M. E. Dinger, M. J. Cowley, Seave: A comprehensive web platform for storing and interrogating human genomic variation. *Bioinformatics* **35**, 122–125 (2019).
91. W. McLaren *et al.*, The ensembl variant effect predictor. *Genome Biol.* **17**, 122 (2016).
92. S. T. D. Team, *SRA Toolkit Development Team* (NCBI, 2023) (https://trace.ncbi.nlm.nih.gov/Traces/sra/sra.cgi?view=software).
93. P. Danecek, *et al.*, Twelve years of SAMtools and BCFtools *Gigascience* **10**, giab008 (2021), 10.1093/gigascience/giab008.
94. J. K. Bonfield, *et al.*, HTSlib: C library for reading/writing high-throughput sequencing data *Gigascience* **10**, giab007 (2021), 10.1093/gigascience/giab007.
95. R. C. Team, *R: A Language and Environment for Statistical Computing in R Foundation for Statistical Computing* (The R Foundation, Vienna, Austria), 2021).
96. P. team, *RStudio: Integrated Development Environment for R in Posit Software* (PBC, Boston, MA, 2022).
97. D. Miao *et al.*, Genomic correlates of response to immune checkpoint blockade in microsatellite-stable solid tumors. *Nat. Genet.* **50**, 1271–1281 (2018).
98. V. Anagnostou *et al.*, Multimodal genomic features predict outcome of immune checkpoint blockade in non-small-cell lung cancer. *Nat. Cancer* **1**, 99–111 (2020).
99. A. M. Wickham *et al.*, Welcome to the Tidyverse. *J. Open Source Soft.* **4**, 1486 (2019).
100. A. T. Marees, *et al.*, A tutorial on conducting genome-wide association studies: Quality control and statistical analysis *Int. J. Methods Psychiatr. Res.* **27**, e1608 (2018), 10.1002/mpr.1608.
101. S. Purcell *et al.*, PLINK: A tool set for whole-genome association and population-based linkage analyses. *Am. J. Hum. Genet.* **81**, 559–575 (2007).
102. B. L. Browning, X. Tian, Y. Zhou, S. R. Browning, Fast two-stage phasing of large-scale sequence data. *Am. J. Hum. Genet.* **108**, 1880–1890 (2021).
103. B. L. Browning, Y. Zhou, S. R. Browning, A one-penny imputed genome from next-generation reference panels. *Am. J. Hum. Genet.* **103**, 338–348 (2018).
104. S. Das *et al.*, Next-generation genotype imputation service and methods. *Nat. Genet.* **48**, 1284–1287 (2016).
105. S. A. Lambert *et al.*, The polygenic score catalog as an open database for reproducibility and systematic evaluation. *Nat. Genet.* **53**, 420–425 (2021).
106. H. Yang, H. Wang, R. Jaenisch, Generating genetically modified mice using CRISPR/Cas-mediated genome engineering. *Nat. Prot.* **9**, 1956–1968 (2014).
107. T. Yamazaki *et al.*, Blockade of B7–H1 on macrophages suppresses CD4+ T cell proliferation by augmenting IFN-gamma-induced nitric oxide production. *J. Immunol.* **175**, 1586–1592 (2005).
108. E. A. Eisenhauer *et al.*, New response evaluation criteria in solid tumours: Revised RECIST guideline (version 1.1). *Eur. J. Cancer* **45**, 228–247 (2009).

Downloaded from https://www.pnas.org by 138.25.168.236 on January 11, 2026 from IP address 138.25.168.236.